Stresses Near a Change of Thickness in a Continuous-Fiber-Composite Plate

Thesis by

Thomas J. Kubr

In Partial Fulfillment of the Requirements for the Degree of

Aeronautical Engineer

Research supported by NASA grant NSG 1483

and the Swiss Academy of Engineering Sciences

California Institute of Technology

Pasadena, California

1990

(submitted June 1, 1990)

I dedicate this thesis to my dear wife Denise,

for her love and support,

and the joy she brought to my life.

Acknowledgments

The research presented in this thesis has been supported by the National Aeronautics and Space Administration through grant NSG 1483. I am very grateful for the generous fellowship awarded to me by the Swiss Academy of Engineering Sciences, because it allowed me to concentrate fully on my research.

A warm thank you goes to my advisor, Prof. Wolfgang Knauss, who kept my thoughts on track and taught me sound scientific reasoning. I very much appreciate the lively discussions with Prof. Heinrich Bergmann and his profound knowledge of composites, as well as the interactions with Profs. J. Knowles, A. Rosakis and J. Hall.

The help from Jean Anderson of the Aero library is acknowledged, as well as Jon Melvin and Tom Welmers for keeping CADRE up and running when I needed it most. Furthermore, I thank Theresa Thalken for her support and friendship.

A special thanks goes to my roommate Jacques Belanger, who patiently listened to my woes with computers, and to my friends and colleagues of the Solid Mechanics Group, Catherine Brinson, Xiaomin Deng, Philippe Geubelle, John Lambros, Tim Minahen, and Guillaume Vendroux, for their help on the numerous little questions that always seem to take the most time to solve.

Abstract

This thesis presents the results of a numerical investigation of the stresses near an abrupt change in thickness of a composite plate. The plate is a laminate of unidirectional, continuous fiber plies. The study is aimed at gaining insight into the failure behavior of co-cured stringer reinforced composite plates and shells.

The analysis is performed in a plane normal to the stringer axis. The problem formulation is similar to plane strain. Because orthotropic materials are involved, a solution method allowing three-dimensional displacements as functions of two spatial variables is applied. The method is called plane-coupled strain. Failure is assumed to initiate at the sharp 90° reentrant corner of the step-down geometry due to a rise in stresses. The resulting stress singularity is characterized for different combinations of stacking orders in the stepped plate. Stresses in the structure are determined by means of the finite element method.

The results are presented in two parts: The first describes the differences obtained with plane-coupled strain and classical plane strain; the second characterizing the stress singularity. The more computer intensive plane-coupled strain solution produces significantly different results for the stresses near the singularity. The character of the stress singularity is found to be highly dependent on the fiber direction of the material at the sharp corner.

The results for the stress singularity are used in an example failure criterion. Stacking sequences are examined with respect to their susceptibility to failure under different combinations of in-plane loading.

Table of Contents

Acknowledgments iv
Abstract v
Table of Contents vi
List of Figures viii
List of Tables ix
1. Introduction 1
2. Coordinate Conventions 3
3. Problem Statement 5
3.1. The Generic Problem: Step-Down of a Composite Plate 5
3.1.1. Motivation 5
3.1.2. The Step-Down Geometry 5
3.2. Boundary Conditions 8
3.2.1. Load Cases 8
3.2.2. Displacement Boundary Conditions 9
3.3. Material Description 9
3.3.1. Model of the Material 9
3.3.2. Model of a Laminate 10
3.3.3. The Constitutive Law 11
3.3.4. Material Constants 13
3.4. Rays into the Singularity 13
3.5. Laminate Stacking Order 14
4. Solution Method 17
4.1. Plane Strain and Composite Materials 17
4.1.1. The Theory of Plane Strain 18
4.1.2. Introducing Composite Materials into Classical Plane Strain Problems. 20
4.1.3. Plane-Coupled Strain 21
4.1.4. Plane-Coupled Strain and the Finite Element Method 23
4.2. Stress Singularity at the Corner 25
4.2.1. The Expected Character of the Solution near the Corner 25
4.2.2. Method 26
5. Results 28
5.1 The Effects of using Plane-Coupled Strain 28
5.1.1. Out-of-Plane Displacement 28
5.1.2. Differences between Classical Plane Strain and Plane-Coupled Strain .. 31
5.1.3. The Differing Nature of the Stress Singularity 34
5.1.4. Summary 35
5.2. The Stress Singularity 36
5.2.1. Isotropic Test Case and Accuracy of the Solution Method 36
5.2.3. The Severity of the Singularity 38
5.2.4. Comparison of Intensity Coefficients 41
5.3. Example of a Failure Criterion 48

6. Suggestions for Future Research 51
6.1. Analytical Analysis 51
6.2. Experimental Work 51
6.3. Improved Numerical Method 51
7. Concluding Remarks 53
Bibliography 55
Appendix I: Computing Tools ..... a
Appendix II: Implementation of Plane-Coupled Strain in Nastran ..... b

List of Figures

Figure 2.1. Coordinate systems 3

Figure 2.2. Material coordinate system 4

Figure 3.1. Examples of composite structures with dropped plies 6

Figure 3.2. Geometry of the problem 7

Figure 3.3. Load cases 8

Figure 3.4. Rays at the Corner 14

Figure 3.5. Plies in stringers 15

Figure 3.6. Plies in an I-type stringer 15

Figure 4.1. Prismatic body suitable for plane strain analysis 17

Figure 4.2. Solid finite element 23

Figure 4.3. Corner in an infinite plate/plane 26

Figure 4.4. Sketch of a stress log-log plot 27

Figure 5.1. Out-of-plane displacement function. Case 3, moment loading 29

Figure 5.2. Out-of-plane displacement function. Case 13, tension loading 29

Figure 5.3. Out-of-plane displacement function. Case 2, shear loading 30

Figure 5.4. Case 2R vs. Case 2 [% difference]; σ_{xx}, tension loading 32

Figure 5.5. Case 3R vs. Case 3[% difference]; σ_{xy}, moment loading 32

Figure 5.6. Case 5, σ_{zx} compared to σ_{xy} [%]; shear loading 34

Figure 5.7. Example log-log stress plot, Case 2, Tension, σ_{ff} 37

Figures 5.8.a - l Intensity coefficients ..... 42 - 47

Figure 5.9. Failure plane and failure normal 49

Figure 5.10. End-points of failure normals 50

List of Tables

Table 3.1. Material Parameters 13

Table 3.2. Stacking Orders 16

Table 5.1. Severities of the Stress Singularity 39

1. Introduction

For decades, metals have been the materials of choice in the construction of transportation vehicles. In general, metals are strong, stiff, tough, formable, and can be used over a wide range of temperatures. Steel provided for durable cars, ships and trains; the world's airline fleet was possible thanks to inexpensive and lightweight aluminum; the mastery of titanium allowed high powered jet engines and hypersonic flight. With the advent of high performance fibers, substantial gains in performance and weight savings became possible in the form of composite materials. However, fiber composites are slow to replace metal structures because of the lack of experience with the damage response and the more complex stress analysis. The improvement in damage characteristics remains in part the domain of material science, but structural engineering can improve the understanding of the stresses in composite structures and their proper use. Better insight into structural problems is still the key to exploit the full advantage of the given material characteristics.

This thesis attempts to aid in understanding the failure of co-cured, stringer reinforced composite plates. Stringers are very efficient in strengthening and stiffening thin plates and shells used in the wings and fuselages of aircraft. Co-curing of the plate and the stringers produces one integral part and seems to provide the best possible bond between plate and stringers. However, the geometric discontinuities at the stringer attachments can give rise to severe stress concentrations that are thought to be responsible for the failure of such plates. Thus, this work attempts to better understand the effect of stress risers at the plate-stringer interface, an understanding that can ultimately be used for safer and more efficient designs.

Failure analysis is inherently dependent on the local stress field. Since structural engineering concentrates on the overall load bearing capabilities of a structure, it is desirable to find methods that characterize failure in terms of the applied loads on the plate. One of the weak points in stringer reinforced plates is the flange termination of the stringer. The stringer termination is equivalent to a change in the thickness of the plate. Thus the generic problem of a step-down in plate thickness is studied in this thesis. The step-down gives rise to high stresses at the reentrant corner between the base plate and the stringer, which in turn are thought to be responsible for failure initiation.

In order to understand the mechanics of failure near the stringer-plate interface, it is necessary to examine the stress field at the corner. One can either choose to employ an arbitrary fillet radius or assume a sharp corner and characterize the resulting stress singularity. A fillet radius can result in a realistic physical problem for metallic structures. However, for composite structures the change in thickness is achieved by terminating fibers, and a controlled curvature becomes impractical. A finite element solution is employed to determine the nature of the stress singularity as a function of the ply stacking order and the applied global loads. The analysis is performed in two-dimensions only, but allows for a restricted, three-dimensional displacement field. Thus, a method has been developed that links typical generalized plate stresses (moment, tension,and shear) to the local stress field. The results obtained can subsequently be used to find a failure criterion in conjunction with an experimental test series.

Composite materials are inhomogeneous by definition. Because of the very small size of the fibers, it is impractical to model the different phases of the material in a macroscopic investigation that addresses structural performance. Thus, a homogeneous material description with properties equivalent to the composite material is used. The laminate properties are not averaged across the plate thickness, but each ply is modeled separately.

2. Coordinate Conventions

To facilitate the following discussion, it is necessary to define coordinate systems. Figure 2.1. depicts the two coordinate systems frequently used. Index notation (x_1, x_2, x_3) is used for theory development, while coordinates x-y-z are used in the problem description and presentation of results.

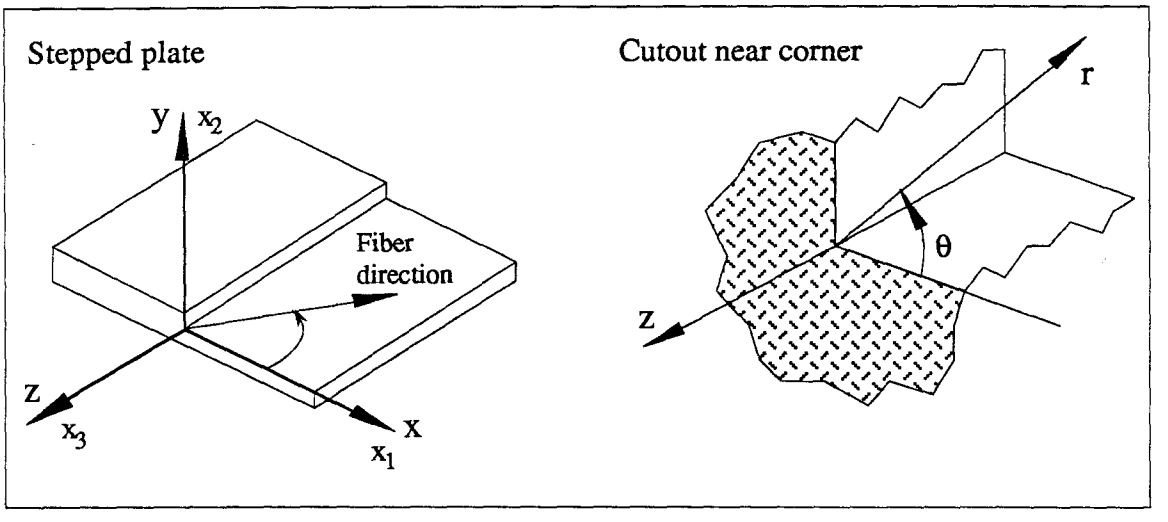

Figure 2.1. Coordinate systems

It should be noted, however, that the Cartesian coordinate system used for the global model of the stepped plate differs from the conventional system used for plates. In this study the coordinate names have been chosen to conform with the convention for plane elasticity. The plane of the plate is formed by the x and z-axes, and the x and y-axes form the plane of analysis.

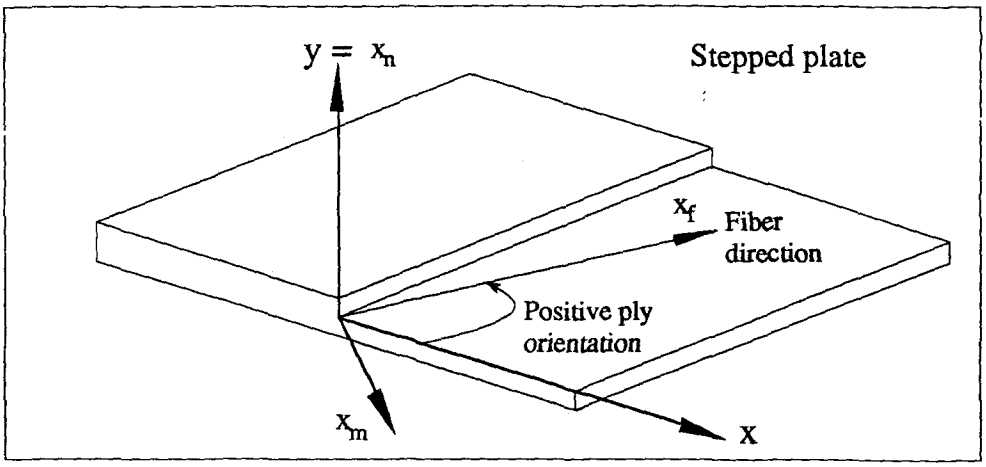

Figure 2.2. Material coordinate system

Ply directions are stated as rotations about the y-axis (figure 2.2.). A ply with fibers parallel to the x-axis is defined as a 0° ply. The sign convention follows the right-hand rule. Results are reported with respect to the material coordinate system x_f, x_m, x_n. The coordinate axis x_f is parallel to the fibers, axis x_n is normal to the plate, and axis x_m is orthogonal to the other two axes and in the plane of the plate.

SI units are used exclusively. The basic unit for length is the mm. The basic unit of force is the N [kg / m s^2], and thus pressure (stress) is given in MPa [N / mm^2].

Certain assumptions of the analysis depend on absolute size scales in the physical problem. Specifically, one ply is assumed to be 0.125 mm thick (standard tape thickness). Graphite fibers are the most commonly used in aerospace applications, and they are assumed here to be the typical fibers with a diameter of 1-3 μm.

3. Problem Statement

3.1. The Generic Problem: Step-Down of a Composite Plate

3.1.1. Motivation

This research is motivated by the failure of co-cured stringer reinforced composite plates. Co-cured plates are the most efficient and most effective option to replace aluminum plates in applications such as wing skins and fuselage panels. Different failure modes have been observed in such plates, many occurring at or near the stringer attachments. It is hoped that an improved understanding of the stresses and strains near the stringer attachment will lead to better and safer designs.

The results presented in this thesis represent the beginning of a research investigation. The purely numerical results may serve as a guide for a follow-on experimental investigation. As a beginning, a better understanding of the stress concentrations near the end of the stringer flange is sought. The problem can be thought of as a thickness change in a plate. Therefore, the first goal of the investigation is a better understanding of the generic problem.

3.1.2. The Step-Down Geometry

The problem of a thickness change in a plate arises in many applications. Stringers attached to a plate, lap joints, or tailored structures (helicopter rotor blades, wing trailing edges) are but a few examples (figure 3.1.). The reentrant corner inherent in all such problems gives rise to a stress amplification. A sharp corner will lead to theoretically

unbounded stresses in linear, small displacement theory. One could also employ a finite filler radius at the corner and thus keep the stresses finite. In metal structures a fillet has load carrying capabilities and can actually be produced. For fiber composites a fillet could only be a hypothetical geometry. Also, the size of the fibers may well be of the same order as the fillet radius; this observation poses questions with regard to the continuity of the material. It was judged that a sharp corner and a characterization of the resulting stress singularity would be better suited for a composite plate.

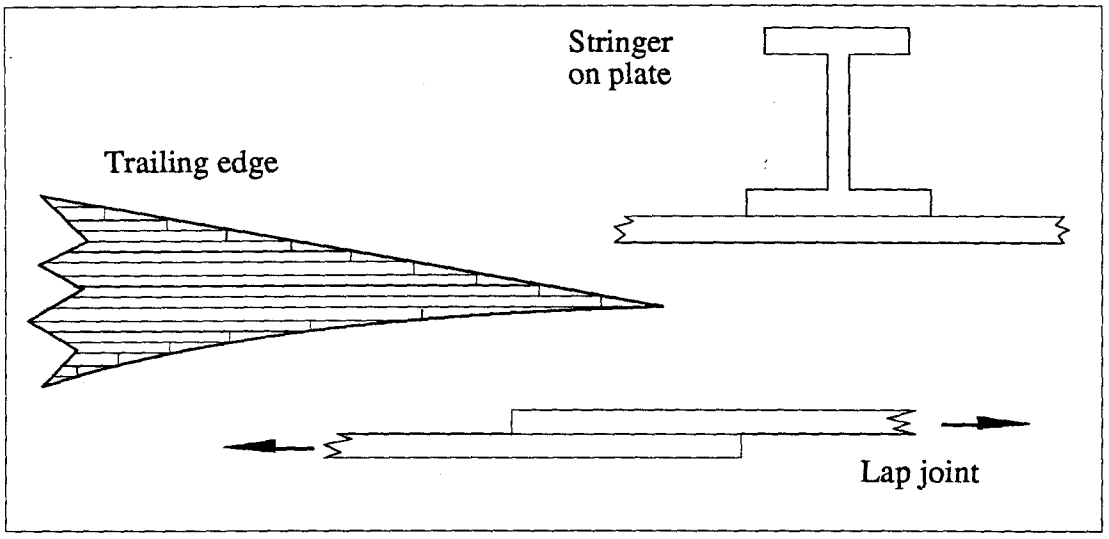

Figure 3.1. Examples of composite structures with dropped plies

There exist a number of possibilities in achieving a change in thickness of a plate. Unlike metals, composite structures do not allow a smooth and continuous change in thickness. The fibers, which are the real load-carrying component of the composite, must be terminated abruptly, which will, in turn, result in finite thickness changes. For practical reasons (manufacturing), whole plies are terminated at once. Some techniques have been suggested that may reduce the effects of the dropped plies (distribution of termination, internal termination, angular shaving of plies at termination). However, these techniques are more expensive to employ. Also, this investigation aims at understanding the physics

underlying the problem of "dropped plies" and should thus be limited to a simple geometry. Thus it is assumed that all plies are terminated at the same location with a cut normal to the plate (figure 3.2.). This geometry is also the easiest and cheapest to manufacture, an important reason for stringer reinforced plates, because of the large number of stringers required.

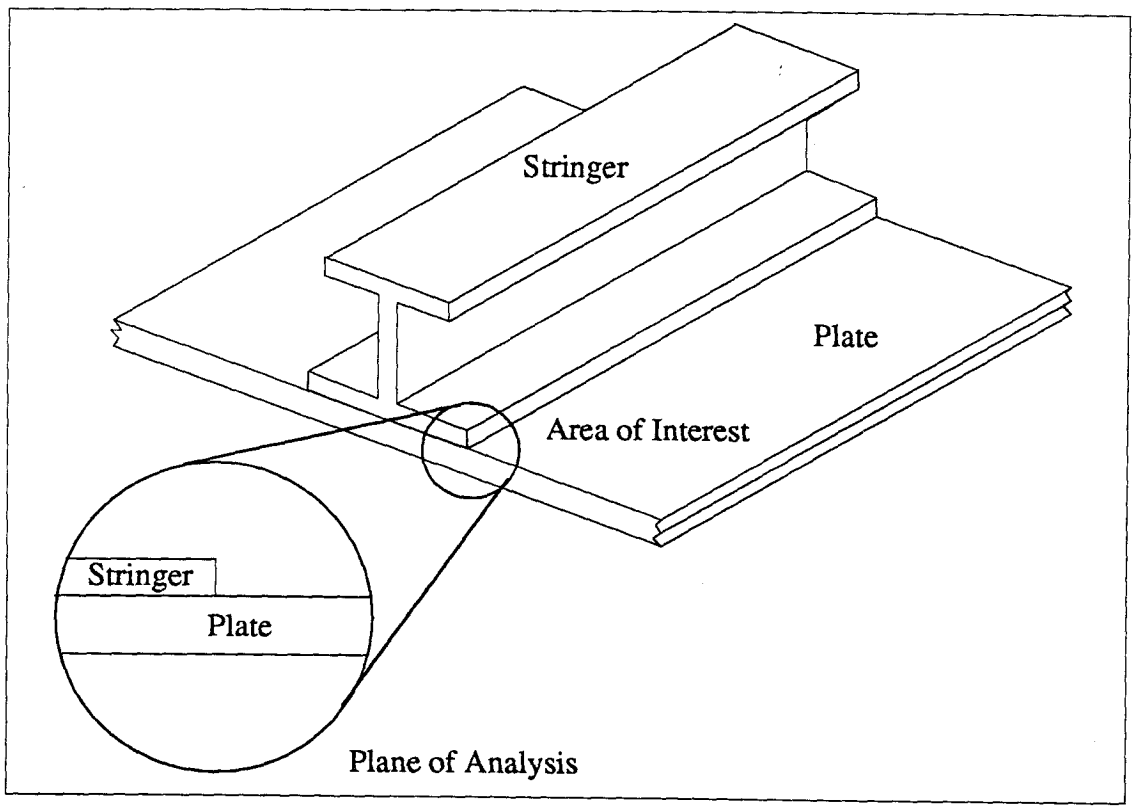

Figure 3.2. Geometry of the problem

The analysis of the problem is performed in a plane (as explained later in section 4.1.). The thickness (and thus the number of plies) of the plate and stringer are variable. Although the analysis is mainly concerned with the behavior at the thickness change, it is necessary to extend the analysis region sufficiently far from the region of interest so that inaccuracies stemming from the application of the boundary conditions diminish (St. Venant).

3.2. Boundary Conditions

3.2.1. Load Cases

Three different load cases are applied to each laminate. Together, they can be superposed to yield results for any in-plane loading condition. Out-of-plane loading has specifically been excluded from the calculations in order to keep the problem manageable. Pure in-plane loading will allow verification of many failure criteria once experimental data becomes available.

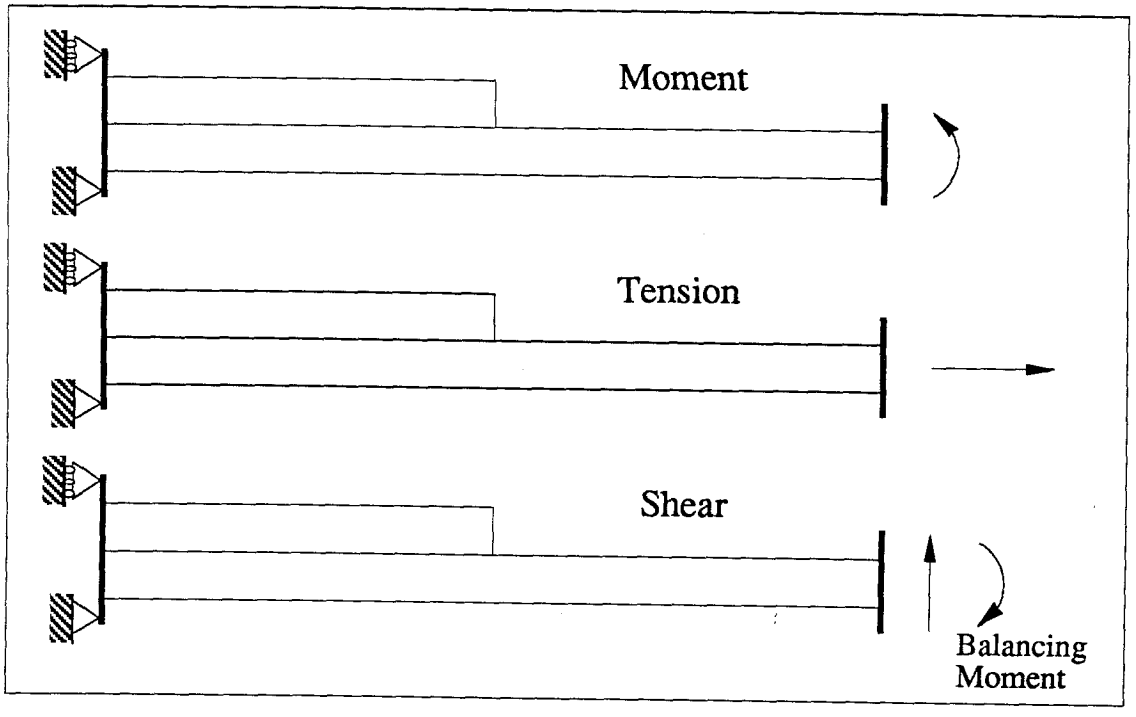

Figure 3.3. Load cases

The three load cases are sketched in figure 3.3. They represent typical generalized plate stresses. The first case is equivalent to a pure bending moment around the z-axis applied to the plate. This case is therefore called the *Moment* load case. The second case (*Tension*) assumes uniform tension in the plate in the x-direction; in this case the moment

resulting from the asymmetric geometry is not balanced. The third case (*Shear*) applies a pure transverse shear. A transverse load at one edge will result however, in a large moment load at the step down. To separate the shear case clearly from the moment case, the transverse load is balanced with an applied moment, such that at the step the net moment will be zero. This combination of transverse and moment loading will result in a pure shear condition at the step. From plate theory it can be seen that the shear load case will exhibit an inflexion point at the step.

3.2.2. Displacement Boundary Conditions

All three loading cases share the same displacement boundary conditions in order to allow superposition of the results. Both model edges are attached to rigid plates (figure 3.3.) and the boundary conditions (both loading and displacement) are applied to the end plates. The displacement condition will introduce an error at the model edges. Thus the model needs to extend far enough for the error to diminish sufficiently near the region of interest (according to St. Venant's principle). The model edges have been chosen to be five to ten plate thicknesses away from the step. Computations have shown that the error vanishes (is no longer detectable) within two laminate (plate + stringer) thicknesses.

3.3. Material Description

3.3.1. Model of the Material

The present study applies to any continuous, parallel fiber composite. Carbon-epoxy has been chosen as a specific material class for this study because of its wide use. Throughout the thesis, the term *composite material* stands for a lay-up of continuous, parallel fiber composite plies. Composite materials are by definition inhomogeneous.

The very small size of the fibers (1-3 μm) makes it impractical to model the different phases of the material. Thus the material properties of the constituents must be suitably combined to yield a homogeneous material with equivalent macroscopic properties.

Composite materials exhibit orthotropic characteristics. One of the planes of orthotropy is normal to the fiber direction. For high quality composites (typical for carbon-epoxy in aerospace applications), the other two orthogonal planes of symmetry can be chosen arbitrarily because the materials are isotropic normal to the fibers. Such materials are called *transversely orthotropic.*

3.3.2. Model of a Laminate

Structures made out of composite materials consist of distinct layers of materials which contain fibers with different orientations. Each such layer is called a *ply*. Each ply is very thin (0.125 mm) and several plies must be combined to obtain thicknesses suitable for structural applications. Stacks of plies are called *laminates.*

Previous studies (Cohen, 1987; Starnes, 1982; Wang, 1984) have averaged the properties of the individual plies across the thickness of the laminate and thus arrived at one homogeneous material for the entire laminate. Some studies differentiated between the material for the plate and the stringer. In this investigation each ply is modeled separately. This approach is believed to lead to a more precise description of the stress singularity at the corner. The properties of the two plies adjacent to the sharp corner will contribute to the nature of the stress singularity, while the plies further away will determine the relation between the globally applied loads (moment, tension, or shear) and the local stress level at the singularity.

Throughout the discussion, the term *inhomogeneous* refers to the laminate, and not the material within each ply. The material in any ply is always modeled as a homogeneous, transversely orthotropic material.

3.3.3. The Constitutive Law

Because the properties of the plies are not averaged over the thickness of the laminate, the constitutive law needs to be developed for a single ply only. Also, since rotation of the material axis is automatically performed by the finite element code, one needs to specify the constitutive law only in the material frame (x_f, x_m, x_n).

An orthotropic material is fully defined by nine independent constants. In terms of engineering constants, the constitutive law reads

$$\{\varepsilon\} = [S]\{\sigma\}$$

$$\begin{Bmatrix} \varepsilon_{11} \\ \varepsilon_{22} \\ \varepsilon_{33} \\ \varepsilon_{12} \\ \varepsilon_{23} \\ \varepsilon_{31} \end{Bmatrix} = \begin{bmatrix} 1/E_1 & -\nu_{12}/E_1 & -\nu_{13}/E_1 & 0 & 0 & 0 \\ & 1/E_2 & -\nu_{23}/E_3 & 0 & 0 & 0 \\ & & 1/E_3 & 0 & 0 & 0 \\ & & & 1/G_{12} & 0 & 0 \\ & \text{sym} & & & 1/G_{23} & 0 \\ & & & & & 1/G_{31} \end{bmatrix} \begin{Bmatrix} \sigma_{11} \\ \sigma_{22} \\ \sigma_{33} \\ \sigma_{12} \\ \sigma_{23} \\ \sigma_{31} \end{Bmatrix}.$$

Because the material is transversely orthotropic, the number of independent constants reduces to five. This condition can be achieved by using the following relations.

$$E_3 = E_2$$

$$\nu_{13} = \nu_{12}$$

$$G_{13} = G_{12}$$

$$G_{23} = G_{23}(E_1, E_2, \nu_{12}, \nu_{23}).$$

In order to enter the material data into the finite element code, the constitutive law must be stated in terms of strains.

$$\{\sigma\} = [C]\{\varepsilon\}$$

$$[C] = [S]^{-1}$$

Inverting [S], one arrives at the following matrix [C] for a transversely orthotropic material:

$$\begin{bmatrix}
\frac{E_1^2(\nu_{23}-1)}{E_1(\nu_{23}-1)+2E_2\nu_{12}^2} & \frac{-E_1E_2\nu_{12}}{E_1(\nu_{23}-1)+2E_2\nu_{12}^2} & \frac{-E_1E_2\nu_{12}}{E_1(\nu_{23}-1)+2E_2\nu_{12}^2} & 0 & 0 & 0 \\
 & \frac{E_2(E_2\nu_{12}^2-E_1)}{(\nu_{23}+1)(2E_2\nu_{12}^2+E_1\nu_{23}-E_1)} & \frac{-E_2(E_2\nu_{12}^2-E_1\nu_{23})}{(\nu_{23}+1)(2E_2\nu_{12}^2+E_1\nu_{23}-E_1)} & 0 & 0 & 0 \\
 & & \frac{E_2(E_2\nu_{12}^2-E_1)}{(\nu_{23}+1)(2E_2\nu_{12}^2+E_1\nu_{23}-E_1)} & 0 & 0 & 0 \\
 & \text{sym} & & G_{12} & 0 & 0 \\
 & & & & G_{23} & 0 \\
 & & & & & G_{31}
\end{bmatrix}$$

The shear modulus G_{23} is determined by the following equation (Jones, 1975):

$$G_{23} = (C_{11} - C_{12})/2$$

$$= \frac{E_1}{2}\left(1 + \frac{E_1\nu_{12}(1-2\nu_{12})}{E_1(\nu_{23}-1)+2E_2\nu_{12}^2}\right)$$

3.3.4. Material Constants

Results obtained in this study are intended to relate to results of a subsequent experimental study. It was thus important to use parameters of a readily available material. T300/BP907 is chosen because it has been used at GALCIT before in specimens supplied by the NASA Langley Research Center, the likely source of specimens for the experimental study. Parameters of an alternate material with stronger orthogonal properties (fiber/matrix stiffness ratio), IM7/8551-7, are used in one case. The known properties of both materials are given in table 3.1. (Waas, 1987). No value for ν_{23} was available and has arbitrarily been taken as 0.33 for T300/BP907 and 0.30 for IM7/8551-7.

Table 3.1. Material Parameters

Material	E_1 [GPa]	E_2 [GPa]	G_{12} [GPa]	ν_{12}	ν_{23}
T300/BP907	111	13.0	6.40	0.38	0.33
IM7/8551-7.	141	6.69	3.17	0.33	0.30

3.4. Rays into the Singularity

In order to study the nature of the singularity at the reentrant corner, stresses along four straight lines (called "rays" from here on) which originate at the corner are collected (figure 3.4.). The rays are chosen to be in the plane of the ply (Ray 1 and Ray 3), or perpendicular to the plies (Ray 2 and Ray 4). Some stress components cannot be used for the results evaluation, either because they are zero (at the free boundaries, Ray 1 and Ray 2), or because there is a material (lamina) interface (Ray 3 for some laminates).

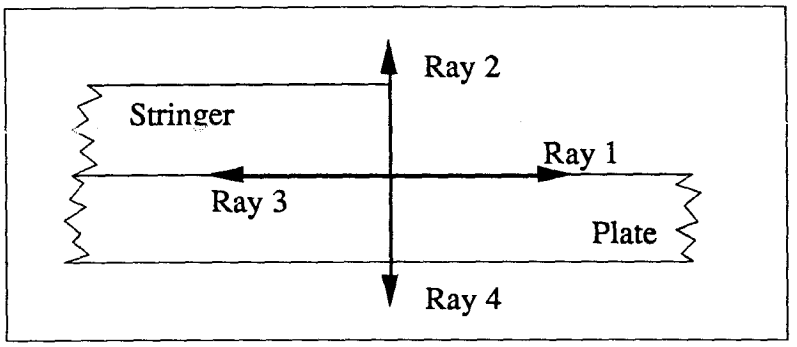

Figure 3.4. Rays at the Corner

3.5. Laminate Stacking Order

A total of 23 different stacking orders have been considered. The different cases are listed in Table 3.2. The table also includes the thickness of the base plate and the step-down thickness ratio. Further, the fiber directions of the plies at the corner are listed separately. The plies at the corner are also referred to as *interface plies* because they form the interface between the stringer and the plate. The stacking orders have been chosen to form an initial data base in order to aid in making decisions for any follow-on experimental testing. One may want to analyze other possibilities after the initial results of the experiments are available.

All base-plate laminates used are quasi-isotropic, symmetric and balanced. The plate is eight plies strong (1.0 mm) for 17 laminates and 16 plies strong (2.0 mm) for the other six laminates. A variety of stacking orders were used for the stringer laminates. Some stringer laminates were also quasi-isotropic, but the majority of the stringer laminates were assumed to be part of a reinforcing mechanism. The assumed stringers are thought to increase the bending stiffness around the x-axis. Thus 90° plies are used either to strengthen the flanges of an I-beam stringer, or as flat strips (figure 3.5.a and b). A combination of ±45° plies is used in the web of an I-beam stringer to obtain high stiffness

in shear (3.5.c). The ±45° plies are usually not terminated at the base of the web, but rather are divided and bent to form part of the flange (figure 3.6.).

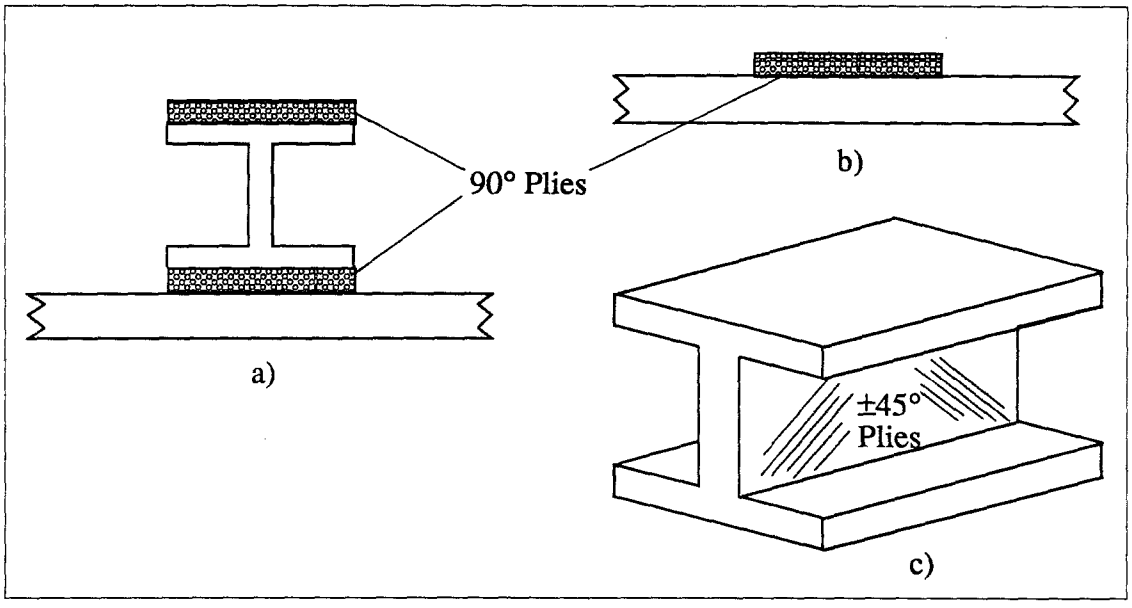

Figure 3.5. Plies in stringers

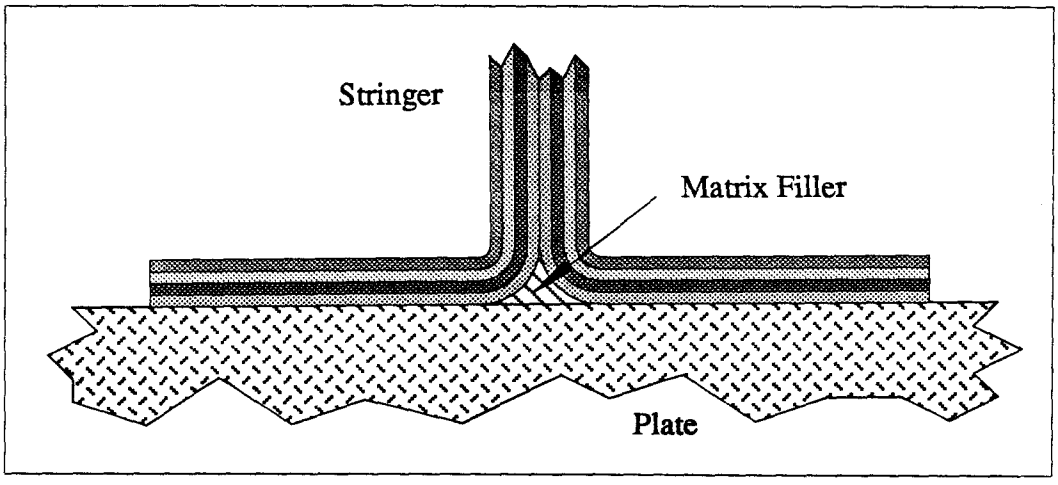

Figure 3.6. Plies in an I-type stringer

Table 3.2. Stacking Orders

Case Identification	Plate Layup	Stringer Layup	Plate Thickness [mm]	Step Ratio	Interface Plate / Stringer
IS	isotropic	isotropic	1.0	2.0	isotropic
1	$[90/0/\pm45]_S$	$[90/0/\mp45]_S$	1.0	2.0	90 / 90
2,2A,2R,2AR	$[90/45/0/-45]_S$	$[90/45/0/-45]_S$	1.0	2.0	90 / 90
3, 3R	$[45/0/-45/90]_S$	$[-45/90/45/0]_S$	1.0	2.0	45 / -45
4	$[90/0/\mp45]_S$	$[\mp45_3/90/0]$	1.0	2.0	90 / -45
5, 5R	$[90/0/\mp45]_S$	$[\mp45/0/90]$	1.0	1.5	90 / -45
6	$[90/0/\mp45]_S$	$[\mp45/\pm45/0/90]$	1.0	1.75	90 / -45
7	$[90/0/\mp45]_S$	$[\mp45]$	1.0	1.25	90 / -45
8	$[90/0/\mp45]_S$	$[90/0/\mp45_3/0/90]$	1.0	2.25	90 / 90
9	$[90/0/\mp45]_S$	$[0/\mp45/90_2]$	1.0	1.625	90 / 0
10	$[90/0/\mp45]_S$	$[\mp45/90_2]$	1.0	1.5	90 / -45
11	$[90/-45/0/45]_S$	$[\mp45/90_2]$	1.0	1.5	90 / -45
12	$[90/-45/0/45]_S$	$[\pm45/\mp45/90_2]$	1.0	1.75	90 / +45
13	$[0/-45/90/45]_S$	$[90_2/\pm45]_S$	1.0	2.0	0 / 90
14	$[0/-45/90/45]_S$	$[90/\pm45]_S$	1.0	1.75	0 / 90
15	$[(0/90)_2/\mp45_2]_S$	$[90/0/\mp45]_S$	2.0	1.5	0 / 90
16	$[(0/90)_2/\mp45_2]_S$	$[90_2/\mp45]_S$	2.0	1.5	0 / 90
17	$[(0/90)_2/\mp45_2]_S$	$[\mp45/90_2]$	2.0	1.25	0 / -45
18	$[(0/90)_2/\mp45_2]_S$	$[90_4]$	2.0	1.25	0 / 90
19	$[(90/0)_2/\mp45_2]_S$	$[90_4]$	2.0	1.25	90 / 90
20	$[90_2/0_2/-45_2/45_2]_S$	$[90_4]$	2.0	1.25	90 / 90
21	$[90/0/\mp45]_S$	$[90_2]$	1.0	1.25	90 / 90
22	$[90/0/\mp45]_S$	[90]	1.0	1.125	90 / 90
23	$[45/0/-45/90]_S$	$[45/0/-45/90]_S$	1.0	2.0	45/45

4. Solution Method

4.1. Plane Strain and Composite Materials

Plane strain assumptions have long been used in structural analysis. Plane strain leads to an exact formulation of a two-dimensional elasticity problem, allowing accurate modeling of stresses, strains and displacements in the interior of an appropriate body under in-plane loading (figure 4.1.). In the past, plane strain assumptions have yielded a great number of useful analytic solutions. Because plane strain does not allow coupling of in-plane and out-of-plane stresses, solutions are generally only valid for isotropic, homogeneous solids. The following section briefly reviews the principals of plane strain in preparation for a choice of deformations appropriate to the problem at hand.

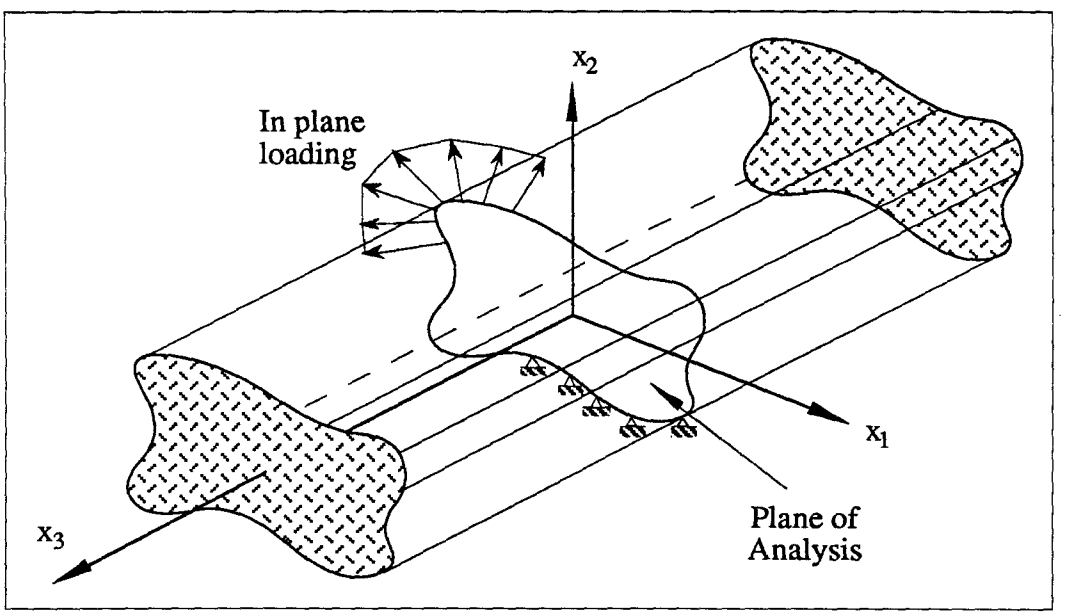

Figure 4.1. Prismatic body suitable for plane strain analysis

4.1.1. The Theory of Plane Strain

Plane strain is based on the following premises:

- There exists no x3-dependence for stress or strain.
- The normal strain in the x_3-direction (ε_{33}) is constant throughout the body.
- There are no body forces acting in the x_3-direction.

These assumptions accurately constrain the field equations of a prismatic body, infinitely long in the x_3 direction. The body is loaded normal to its generators only, without variance in the x_3-direction (figure 4.1.). Plain strain can also be used for stations in the interior of a finite length prismatic body, which are sufficiently removed from the end surfaces (St. Venant's Principle). Thus one can identify the spatial dependence of the field quantities

$$u_1 = u_1 (x_1 , x_2)$$

$$u_2 = u_2 (x_1 , x_2)$$

$$\varepsilon_{ij} = \varepsilon_{ij} (x_1 , x_2)$$

$$\sigma_{ij} = \sigma_{ij} (x_1 , x_2).$$

If, in accordance with typical practice, we further set $\varepsilon_{33} = C$ = constant, integration of ε_{33} yields

$$u_3 = C x_3 + A (x_1 , x_2).$$

The function $A (x_1 , x_2)$ represents an *out-of-plane displacement function.* At this point, plane strain assumptions would set $A (x_1 , x_2)$ equal to zero. For the present study, the

out-of-plane displacement function is of interest and it will be retained for the following discussion. Using $\varepsilon_{ij} = 1/2\,(u_{i,j} + u_{j,i})$, one can write the displacement-strain relations as

$$\varepsilon_{11} = u_{1,1}$$

$$\varepsilon_{22} = u_{2,2}$$

$$\varepsilon_{33} = C$$

$$\varepsilon_{12} = \varepsilon_{21} = {}^1/_2\,(u_{1,2} + u_{2,1})$$

$$\varepsilon_{23} = \varepsilon_{32} = {}^1/_2\,A_{,2}$$

$$\varepsilon_{31} = \varepsilon_{13} = {}^1/_2\,A_{,3}.$$

Introducing the constitutive law for an isotropic, homogeneous body using the Lamé constants, one obtains the following stress-strain relations.

$$\sigma_{11} = (\lambda + 2\,\mu)\,u_{1,1} + \lambda\,u_{2,2} + \lambda\,C$$

$$\sigma_{22} = (\lambda + 2\,\mu)\,u_{2,2} + \lambda\,u_{1,1} + \lambda\,C$$

$$\sigma_{33} = (\lambda + 2\,\mu)\,C + \lambda\,(u_{1,1} + u_{2,2})$$

$$\sigma_{12} = \mu\,(u_{1,2} + u_{2,1})$$

$$\sigma_{23} = \mu\,A_{,2}$$

$$\sigma_{31} = \mu\,A_{,3}.$$

Thus the shearing components σ_{23}, σ_{31}, ε_{23}, and ε_{31} are independent of the other components. Further, σ_{33} depends on the in-plane components solely through Poisson's ratio, while ε_{33} is known. Therefore neither enters the solution for the in-plane components (σ_{11}, σ_{22}, σ_{12} and ε_{11}, ε_{22}, ε_{12}).

In the classical plane strain case for isotropic solids, the out-of-plane displacement A (x_1 , x_2) is set equal to zero. Problems such as anti-plane shear or twist of prismatic, isotropic bodies represent the complement to plane strain problems. For these cases, the body is loaded out-of-plane, and the resulting deformation will also be purely out-of-plane. In effect, such problems determine the out-of-plane displacement function A (x_1 , x_2) and the shear component σ_{23}, σ_{31}, ε_{23}, and ε_{31}. The solutions for the in-plane and out-of-plane components of appropriate bodies can be determined separately for any combination of in-plane and out-of-plane loading; they are *decoupled.*

4.1.2. Introducing Composite Materials into Classical Plane Strain Problems

If anisotropic materials are introduced into classical plane strain problems, decoupling is in general no longer possible. For example, with orthotropic materials (e.g., composites), decoupling occurs only when one of the material axes is orthogonal to the plane of analysis (0° or 90° plies). To illustrate the coupling effect, let us look at the constitutive law for an orthotropic material. If the material coordinate system of an orthotropic material coincides with the x_1-x_2-x_3 coordinate system, the constitutive law reads in matrix form:

$$\begin{Bmatrix} \sigma_{11} \\ \sigma_{22} \\ \sigma_{33} \\ \sigma_{12} \\ \sigma_{23} \\ \sigma_{31} \end{Bmatrix} = \begin{bmatrix} a_{11} & a_{12} & a_{13} & 0 & 0 & 0 \\ & a_{22} & a_{23} & 0 & 0 & 0 \\ & & a_{33} & 0 & 0 & 0 \\ & & & a_{44} & 0 & 0 \\ & \text{sym} & & & a_{55} & 0 \\ & & & & & a_{66} \end{bmatrix} \begin{Bmatrix} \varepsilon_{11} \\ \varepsilon_{22} \\ \varepsilon_{33} \\ \varepsilon_{12} \\ \varepsilon_{23} \\ \varepsilon_{31} \end{Bmatrix}.$$

Since all components in the upper right quadrant are zero, the out-of-plane shear components σ_{23}, σ_{31}, ε_{23}, and ε_{31} are decoupled from the in-plane components, and thus

the out-of-plane displacement function A (x_1 , x_2) does not enter the solution. However, if the material axes are rotated out of the plane of analysis, the constitutive law will change as a result of the rotation around the x_2-axis (*in-plate* rotation).

$$\begin{Bmatrix} \sigma_{11} \\ \sigma_{22} \\ \sigma_{33} \\ \sigma_{12} \\ \sigma_{23} \\ \sigma_{31} \end{Bmatrix} = \begin{bmatrix} b_{11} & b_{12} & b_{13} & 0 & 0 & b_{16} \\ & b_{22} & b_{23} & 0 & 0 & b_{26} \\ & & b_{33} & 0 & 0 & b_{36} \\ & & & b_{44} & b_{44} & 0 \\ & \text{sym} & & & b_{55} & 0 \\ & & & & & b_{66} \end{bmatrix} \begin{Bmatrix} \varepsilon_{11} \\ \varepsilon_{22} \\ \varepsilon_{33} \\ \varepsilon_{12} \\ \varepsilon_{23} \\ \varepsilon_{31} \end{Bmatrix}$$

The relation between the matrix components and the rotation angle can be found in many text books, for example Lekhnitzkii (1963). In this case, the solution of the in-plane components clearly depends on the out-of-plane displacement function A (x_1 , x_2).

The above two examples illustrate clearly that, despite appropriate geometry and loading, classical plane strain cannot in general be used for fiber composite laminates. Therefore a solution method is needed that couples the out-of-plane displacement function to the in-plane components.

4.1.3. Plane-Coupled Strain

Since the geometry of the plate step-down problem can be formulated in terms of the spatial variables x_1 and x_2, and because the incorporation of composites prohibits the use of classical plane strain, an expanded two-dimensional theory was used. Since this theory retains the mathematical two-dimensional aspect of plane strain, but allows for coupling of in-plane and out-of-plane components, it is called *Plane-Coupled Strain* Theory. The following paragraphs describe the assumptions of plane-coupled strain.

Plane-coupled strain can be thought of as the "plane strain theory for composite materials". It allows analysis in only two spatial variables, while admitting three displacement components. The theory of plane-coupled strain assumes the displacement field

$$u_1 = u_1(x_1, x_2)$$

$$u_2 = u_2(x_1, x_2)$$

$$u_3 = u_3(x_1, x_2).$$

A constant strain ε_{33} in the body can be included by adding a term Cx_3 to u_3. Also, the boundary conditions are not allowed to vary with x_3, and the body geometry must follow the same restrictions as for plane strain. For isotropic solids and orthotropic solids, for which the planes of material symmetry coincide with the coordinate planes, this theory also provides the stresses and strains accurately and completely and can be used to formulate both plane strain and out-of-plane problems (anti-plane shear, twist) simultaneously.

For inhomogeneous, anisotropic bodies, plane-coupled strain can involve inaccuracies. For composite plates specifically, the laminate must be symmetric and balanced; otherwise, the plate could twist or bend with respect to the x_1-axis, and neither displacement is admissible under the assumptions of plane-coupled strain. Furthermore, plane-coupled strain allows the inclusion of some types of out-of-plane loading (e.g., shear in the plane of the plate). This possibility has not been explored in this work. No attempt has been made to obtain analytical solutions for plane-coupled strain. Instead, a finite element description was sought for immediate use in the plate step-down problem.attempt has been made to obtain analytical solutions for plane-coupled strain.

4.1.4. Plane-Coupled Strain and the Finite Element Method

Since plane-coupled strain admits displacements in the x_3-direction, a typical plane strain element will not suffice. One could either define a new element or use a three-dimensional element, properly constrained, to simulate the new element. The latter course was chosen. The following section describes how a three-dimensional element is constrained to conform with the assumptions of plane-coupled strain.

Figure 4.3. depicts an eight noded solid element. Nodes 101 through 104 lie in the x_1-x_2 plane (back), and nodes 201 through 204 in the x'_1-x'_2 plane (front). The x'_1-x'_2 plane is parallel to and off-set from the x_1-x_2 plane by a distance t . In theory, t can be chosen arbitrarily, but in practice t must be chosen to conform with the aspect ratio limitations of the element. Nodes 101 and 201 have the same X and Y coordinates and are called a *corresponding pair*. The same holds for nodes 102 and 202, 103 and 203, and all other node pairs in the model.

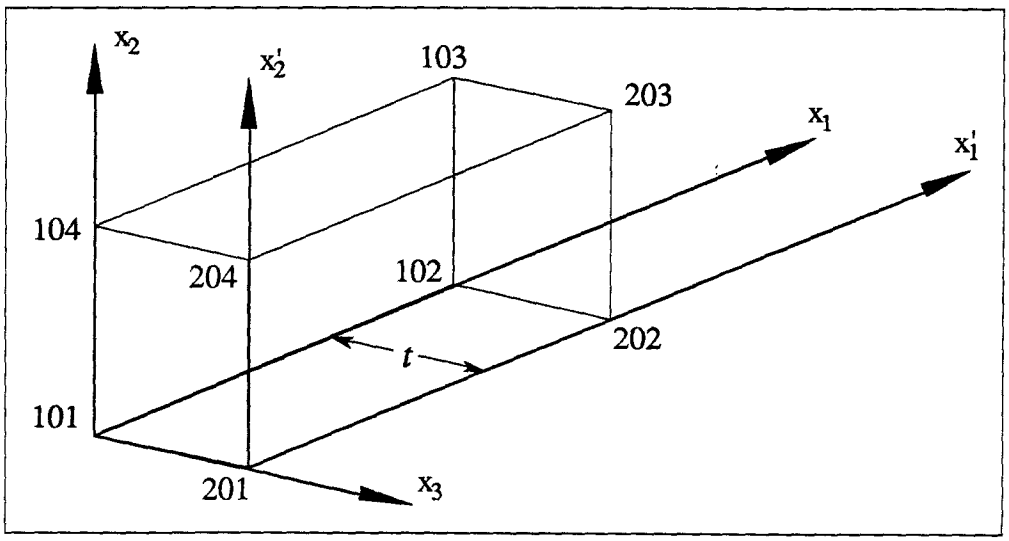

Figure 4.2. Solid finite element

Each node of the element has three degrees of freedom. Constraints are applied to the movement between the two nodes of a corresponding pair, enforcing the assumptions of plane-coupled strain. No restrictions are placed on the movement of the pair as a whole. Because all the field variables are functions of x_1 and x_2 only, each corresponding pair is constrained such that both nodes have the same displacement in the x_1 and x_2 coordinate directions. Displacement in the x_3 direction is constrained such that the difference between the two nodes is constant. This holds true for all corresponding pairs.

$$u_3\,(201) - u_3\,(101) = \Delta t = \text{constant}$$

$$u_3\,(202) - u_3\,(102) = \Delta t = \text{constant}$$

$$u_3\,(203) - u_3\,(103) = \Delta t = \text{constant},$$

etc.

The constant Δt is related to the element thickness t and the strain ε_{33} by

$$\Delta t / t = \varepsilon_{33} = C.$$

The constraints between corresponding nodes are enforced by supplying the finite element code with additional equations, which will delete degrees of freedom from the solution matrix.

When all movement in the x_3-direction is constrained, the element will behave according to classical plane strain assumptions. This fact can be used to determine the difference between a plane strain solution and plane-coupled strain.

4.2. Stress Singularity at the Corner

The sharp reentrant corner at the step-down of the plate will exhibit a stress singularity. The nature of the singularity could be used in a failure criterion. An analytic solution has been provided by M. L. Williams, that is valid for a corner in an isotropic, homogeneous, infinite plate (Williams, 1952). Several different schemes have been proposed to arrive at solutions for a reentrant corner with an orthotropic material; some schemes also include a material interface at the corner (Cohen, 1987). None of the proposed methods are applicable to this research, because they do not provide for the consequences of plane-coupled strain. Since this study is based on a finite element solution for the stress state in the body, the method employed to determine the nature of the singularity is based on results from the finite element calculations.

4.2.1. The Expected Character of the Solution near the Corner

The solution provided by Williams (1952) for an isotropic plate/plane is used as a guide for the solution to the present problem. The geometry of a corner in an infinite plate is illustrated in figure 4.3. The angle of the reentrant corner is given by φ. For r asymptotically approaching zero, the stress components are given by

$$\sigma_{ij} = \Psi_{ij}(\theta)\, r^{-k}.$$

The Ψ_{ij}'s are called *intensity coefficients* in this thesis, and k is called the *severity* of the singularity. For an isotropic material, the severity k depends on the angle of the corner and the boundary conditions at the edges but is independent of material parameters and the angular position θ.

For orthotropic materials (possibly including a material interface), the solution is still expected to follow the same relation, but the severity k can no be longer assumed to be independent of the material properties. It was also found that k is dependant on θ. The following section describes the method used in this study to determine the Ψ_{ij}'s and k.

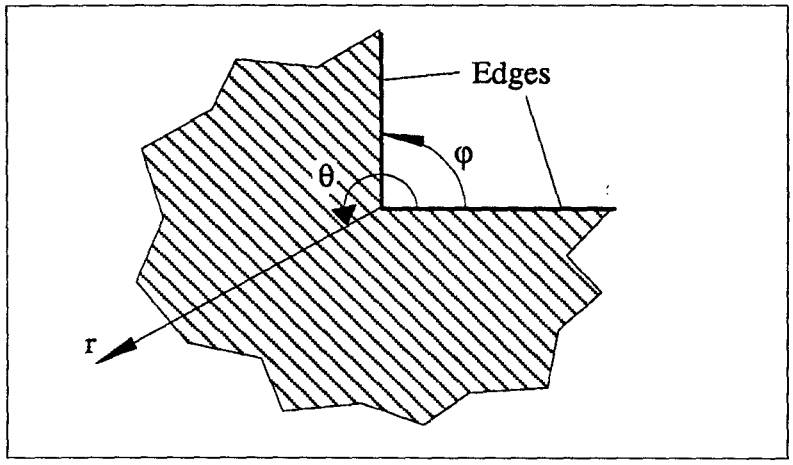

Figure 4.3. Corner in an infinite plate/plane

4.2.2. Method

The stresses at the corner will approach the assumed solution asymptotically as r approaches zero. Therefore, it is necessary to properly scale the region of interest with respect to the overall size of the geometry. The method used to determine the severity k and intensity coefficients of the singularity relies on a very fine finite element mesh near the corner, capable of resolving stresses over several magnitudes of size scale. It is important to note that the resolution of the finite element mesh is carried much farther than is physically sensible. The only purpose of the very fine mesh is to determine the character of the singularity, and no claim on the physical reality of the stresses close to the corner is made.

Stress plotted on a log-log scale along lines of constant θ (*rays*) should appear as a straight line with slope -k (the severity of the stress singularity) and a zero offset of log Ψ (the intensity coefficient). Both k and Ψ are determined by fitting a straight line to the log-log stress data. Figure 4.4. shows a sketch of a log-log stress plot. The portion of the graph corresponding to the elements closest to the corner deviates from the straight line due to the breakdown of the numerical solution. Farther away, the graph deviates because the stress field is not dominated by the singularity. Thus only the center portion of the graph can be used for determining k and Ψ. The quality of this solution method is discussed along with the results of the investigation in section 5.2.1.

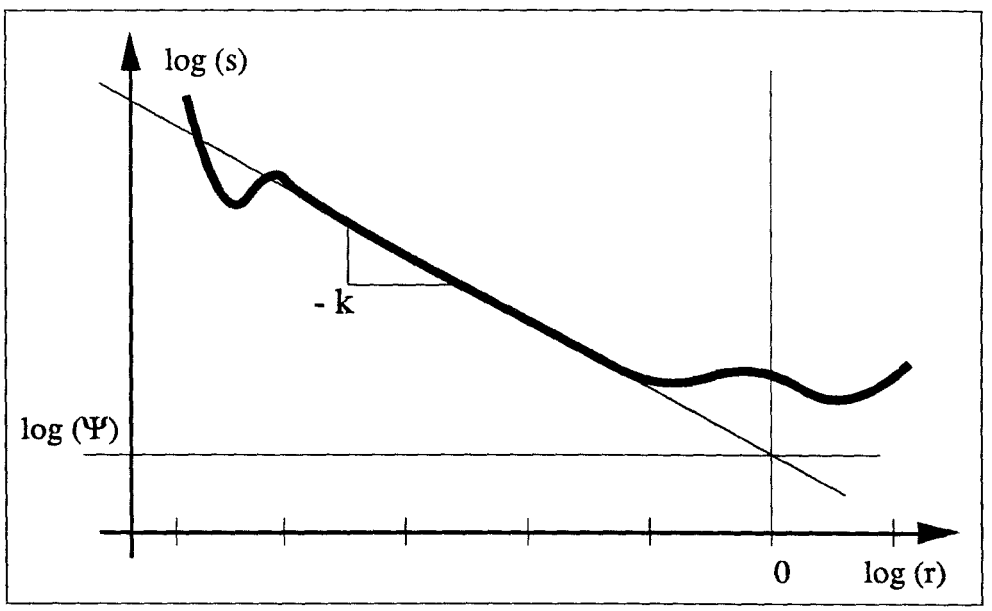

Figure 4.4. Sketch of a stress log-log plot

5. Results

The presentation of results is divided into three parts. Section 5.1. compares plane-coupled strain with classical plane strain results. Section 5.2. discusses the results for the stress singularity at the reentrant corner. Finally, section 5.3. presents one possible way of using the data obtained to link the globally applied loads to a local failure criterion for the stress singularity.

5.1 The Effects of using Plane-Coupled Strain

This section discusses the merits of using plane-coupled strain versus classical plane strain. Results from finite element calculations employing plane-coupled strain are compared with results for identical geometries and loading conditions but with the out-of-plane displacement set to zero (classical plane strain assumptions). Three different stacking orders have been examined using both classical plane strain and plane-coupled strain assumptions. First, plots of the out-of-plane displacements are presented. They portray the overall behavior of the laminate under plane-coupled strain. Second, stresses in the body obtained with plane-coupled strain and classical plane strain are compared. Third, the changing nature of the stress singularity at the reentrant corner is discussed. (This last part uses data that is presented in more detail in the following section, 5.2.)

5.1.1. Out-of-Plane Displacement

The three typical figures presented here, figures 5.1, 5.2, and 5.3, show qualitative plots of the surface topology of the out-of-plane displacement function A (x_1 , x_2) for three different combinations of stacking orders and loading conditions.

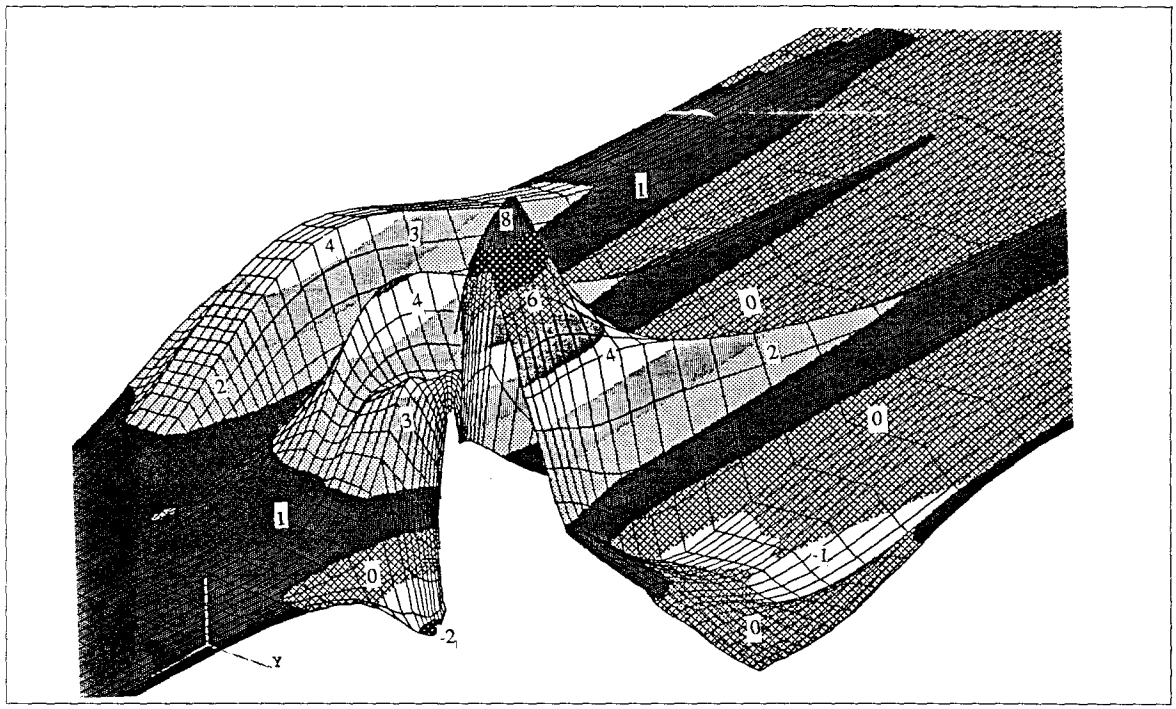

Figure 5.1. Out-of-plane displacement function; Case 3, moment loading; Stacking orders: Plate $[+45/0/-45/90]_S$, Stringer [-45/90/+45/0/0/+45/90/-45]

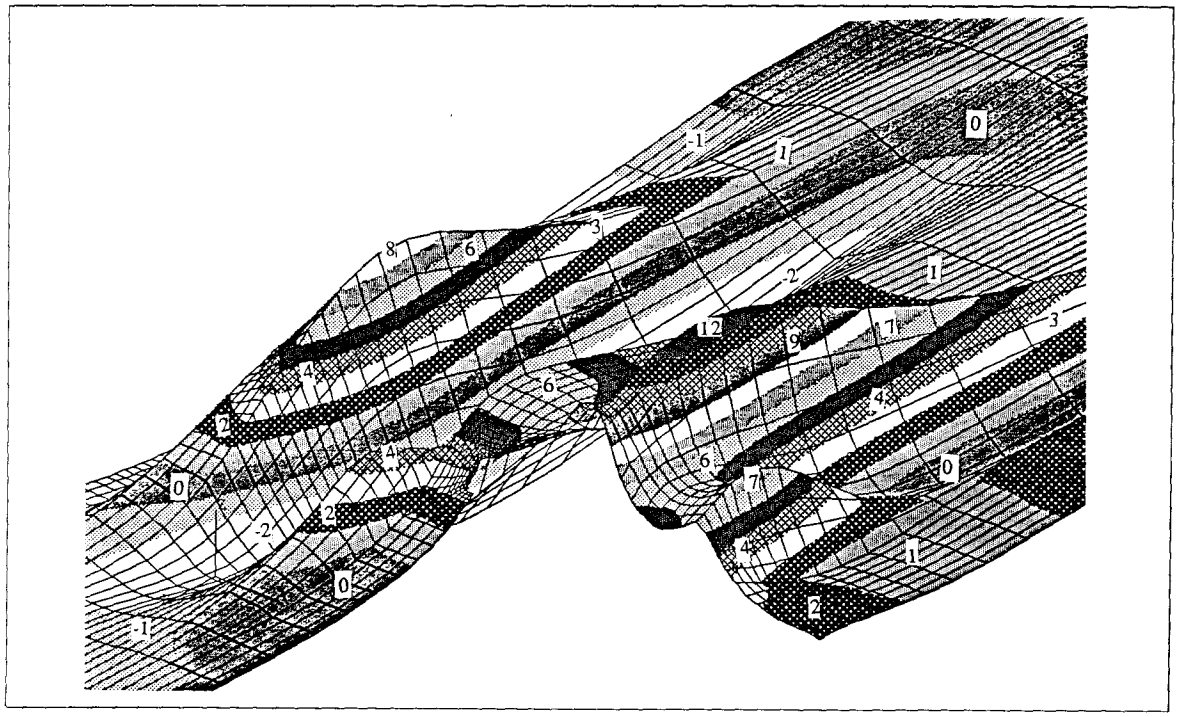

Figure 5.2. Out-of-plane displacement function; Case 13, tension loading; Stacking orders: Plate $[0/-45/90/+45]_S$, Stringer [90/90/+45/-45/-45/+45/90/90]

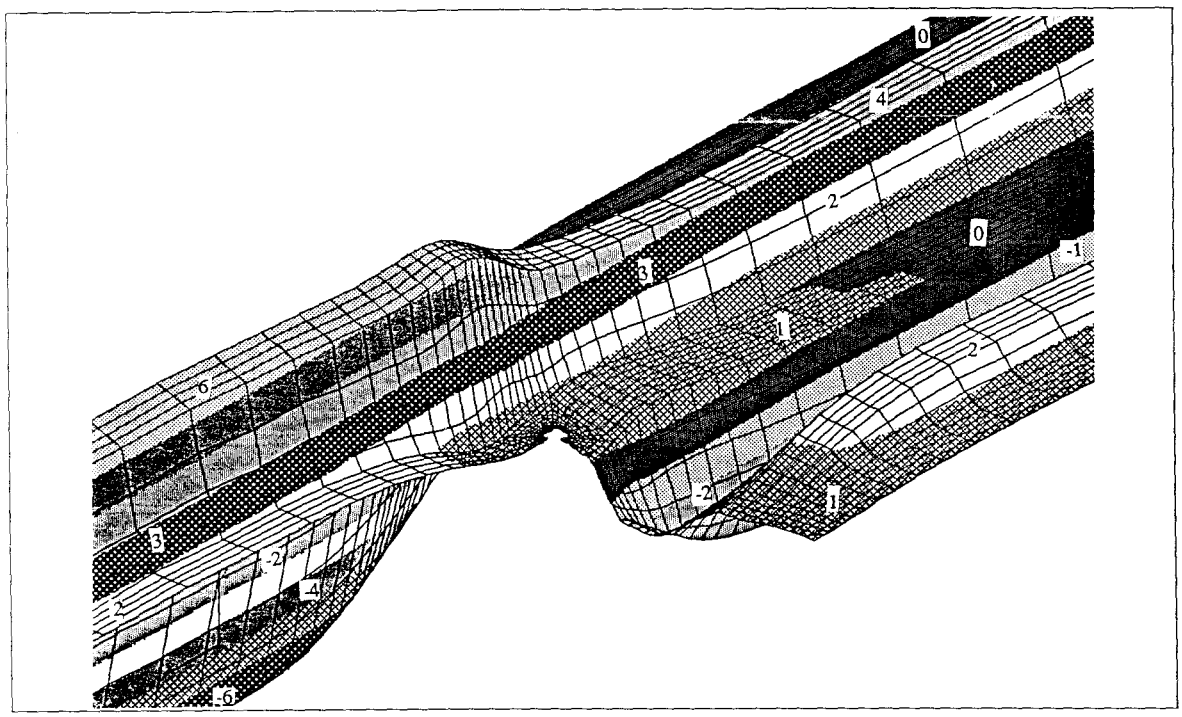

Figure 5.3. Out-of-plane displacement function; Case 2, shear loading; Stacking orders: Plate $[90/+45/0/-45]_S$, Stringer [90/+45/0/-45/-45/0/+45/90]

The mesh on the figures is the finite element mesh used for the analysis. Each ply has been divided into four elements through the thickness. This particular view angle was chosen to best display the area around the corner. The shading levels on the graphs correspond to equal u_3-displacement levels, and the numbers indicate relative displacement magnitudes. The three figures collectively represent the phenomena that have been observed in a number of such plots. All cases (stacking orders) in this study assume a zero axial strain ϵ_{zz}. Therefore the plots are equivalent to the u_3-displacements. The following phenomena deserve special attention:

- Only ±45° plies give rise to u_3-displacements and u_3-displacement gradients. The high gradients give rise to high shear stresses σ_{23} and σ_{31}. Displacement gradients are especially high at +45° / -45° interfaces.

- For the moment and tension load cases, A (x_1 , x_2) tends to zero away from the step. For the shear load case, A (x_1 , x_2) is non-zero and constant with respect to x_1 away from the step. Whether the out-of-plane displacement function tends to zero in an undisturbed stress field (away from the step) depends on the components of the stress field itself. For example, in-plane shear is coupled with out-of-plane shear through the constitutive law and will, in turn, affect the function A (x_1 , x_2). It can be expected that any disturbance on the laminate will give rise to out-of-plane shear stresses σ_{23} and σ_{31}. Attachments, holes, or lateral loads will produce this effect and could all cause the laminate to fail internally.

- At the free edge where the stringer plies are terminated, the largest displacement gradients do not necessarily occur at the edge itself but somewhat inside of the body. Thus free edge delaminations could initiate internally at a ply interface.

- For some cases (figures 5.1. and 5.2), the reentrant corner can be loaded in anti-plane shear, similar to mode III cracks.

Although these phenomena are interesting in and of themselves, they need to be quantified in order to judge their impact on the accuracy of the solution.

5.1.2. Differences between Classical Plane Strain and Plane-Coupled Strain

This section describes the differences in stresses over the entire body. Two figures, 5.4. and 5.5., show the percentage difference for two stress components. Figure 5.6. displays the size of one of the out-of-plane shear components (σ_{31}) with respect to the in-plane shear σ_{12}. The figures show the area immediately around the step. The "mesh" on the figures is not the finite element mesh but a representation of the plies.

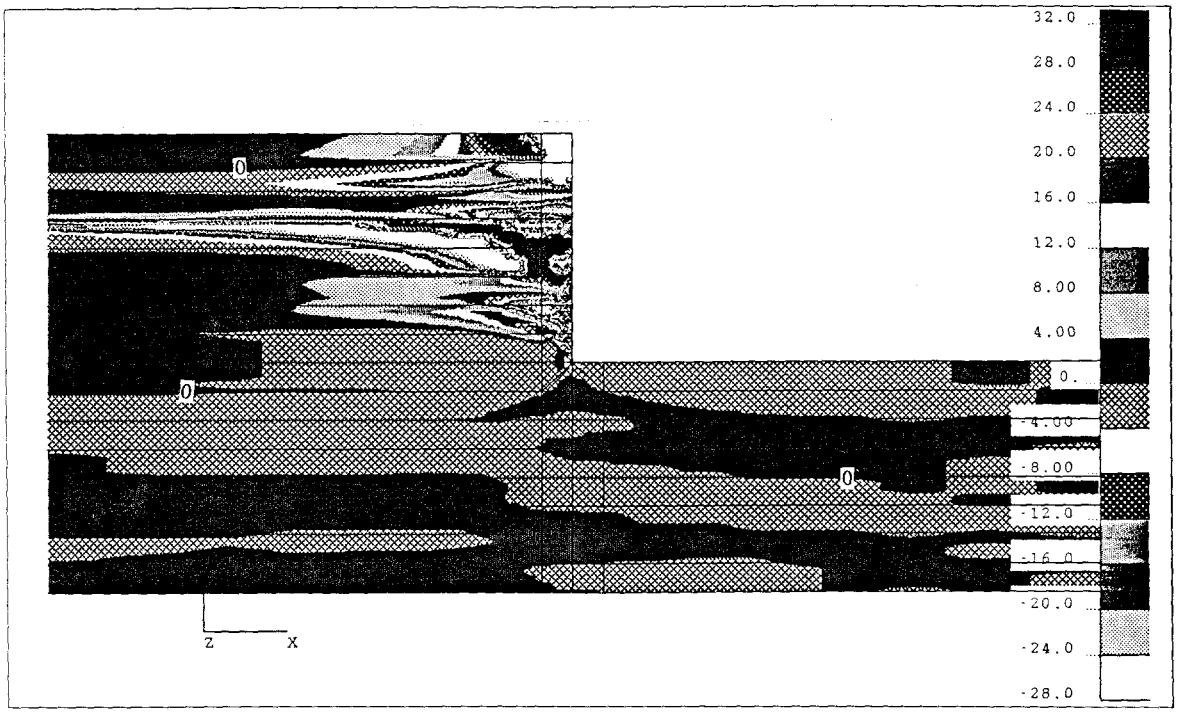

Figure 5.4. Case 2R vs. Case 2 [% difference]; σ_{xx}, tension loading;
Stacking orders: Plate $[90/45/0/-45]_S$; Stringer [90/0/-45/+45/+45/-45/0/90]

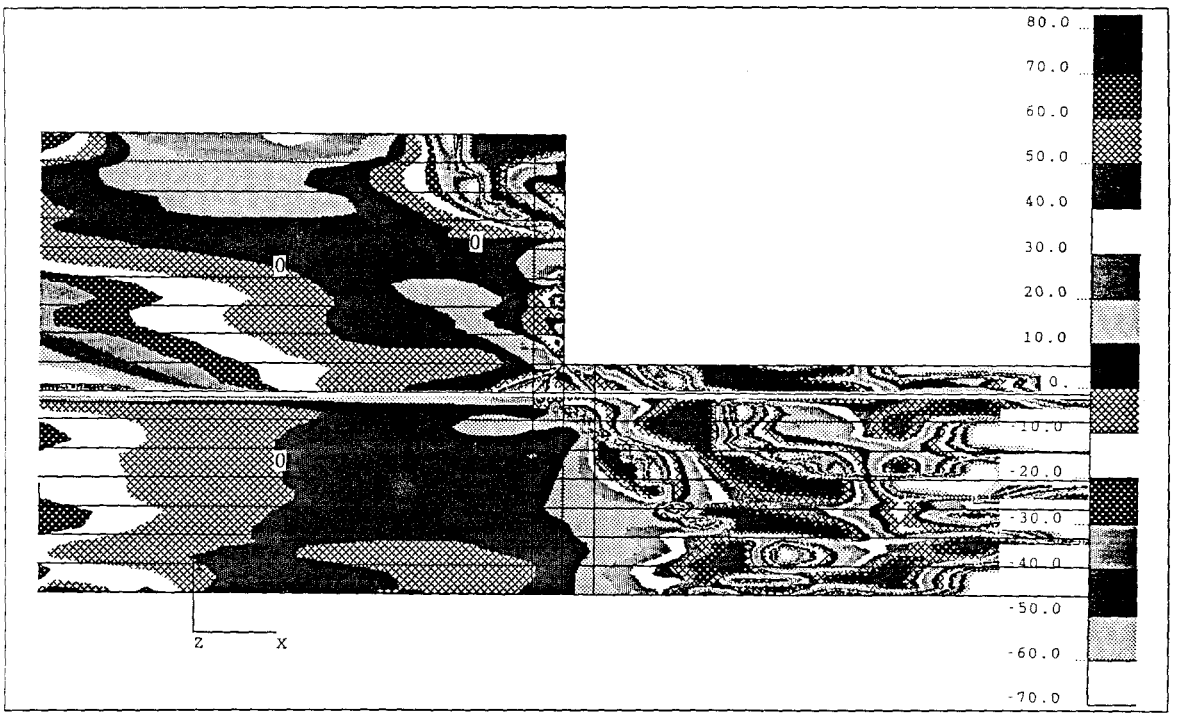

Figure 5.5. Case 3R vs. Case 3 [% difference]; σ_{xy}, moment loading;
Stacking orders: Plate $[+45/0/-45/90]_S$; Stringer [-45/90/+45/0/0/+45/90/-45]

The solution using plane-coupled shear is taken as the reference solution, because it is the more accurate stress formulation. Figures 5.4 and 5.5 display the percentage deviation of the classical plane strain solution with respect to the plane-coupled strain solution. Only in-plane stress components (σ_{xx}, σ_{yy}, σ_{xy}) and σ_{zz} can be compared since the out-of-plane shear stresses, σ_{zx} and σ_{zy}, are identically zero for classical plane strain. The two figures are representative of several more plots produced. In principal, the difference in stresses is small. One must be careful not to interpret the apparently large percentage differences in some areas as large error. For example, the plate portion in figure 5.5 shows large differences. However, since the plate is loaded by a pure moment, the shear stress in the plate should be exactly zero. Thus, the apparent differences in the plate portion can be attributed to inaccuracies in the finite element solution, greatly exaggerated because the data is close to zero. The same holds true for the stresses near the free edges. Areas of nonzero stresses show small differences, see for example the σ_{xx} stresses in the plate portion of figure 5.4. In summary, one notes that a plane-coupled strain solution is not expected to differ from a classical plane strain solution by more than 5% for the in-plane stresses (σ_{xx}, σ_{yy}, σ_{xy}) and σ_{zz}. (This statement is valid only for the global stress field. At the stress singularity, the differences can be greatly amplified, as shown later.)

The merits of using plane-coupled strain become more apparent in figure 5.6. Here the out-of-plane shear stress σ_{zx} is plotted as a percentage value of the in-plane shear σ_{xy} at the same location. Again, the results near free edges are erroneous because the in-plane shear is theoretically zero. For $\pm 45°$ plies, the out-of-plane shear stress is comparable in size with the in-plane shear and certainly cannot be neglected.

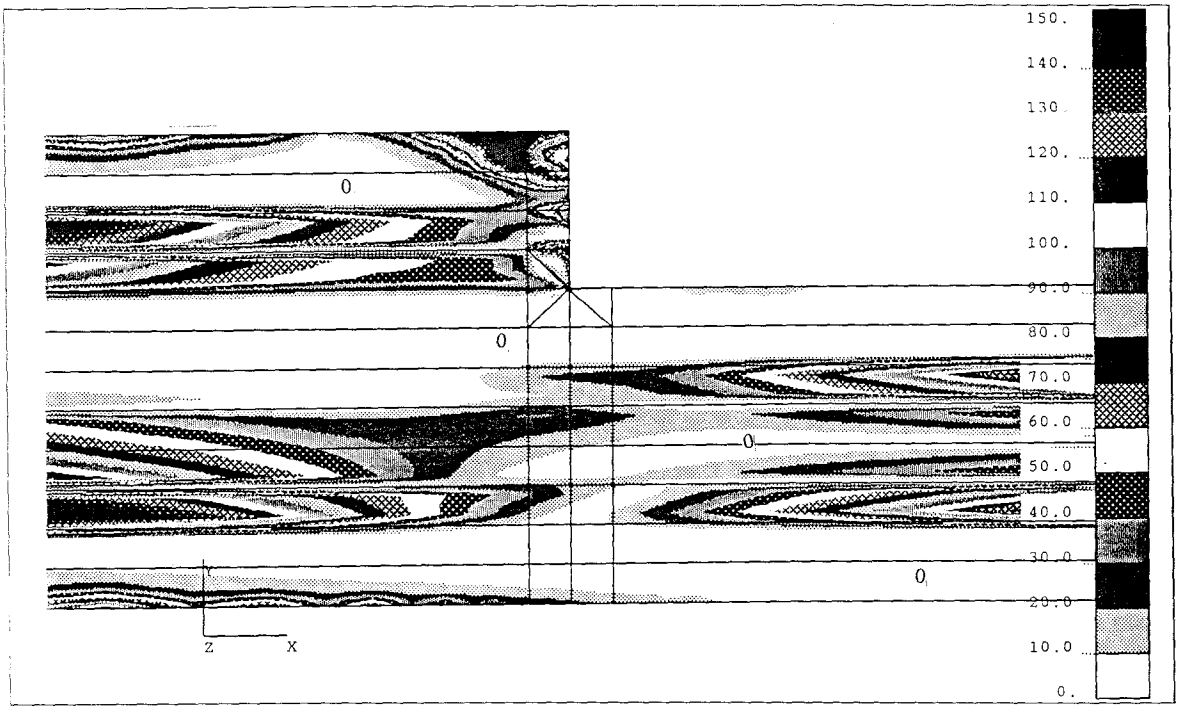

Figure 5.6. Case 5, σ_{zx} compared to σ_{xy} [%]; shear loading;
Stacking orders: Plate [90/0/-45/+45]$_S$; Stringer [-45/+45/0/90]

5.1.3. The Differing Nature of the Stress Singularity

This section refers to data discussed in detail in the following chapter. The reader may chose to come back to this section later.

With respect to the intensity coefficients, the principal difference between the stacking orders is the type of ply interface at the corner. Case 2 has no interface at the corner and the plies are orthogonal to the plane of analysis. Case 3 has a +45° / -45° interface at the corner, while case 5 has a 90° / -45° interface. For case 2, an alternate material with stronger orthogonal material characteristics has also been considered, called case 2A. The cases following classical plane strain assumptions are marked with an R (restricted). The intensity coefficients for all cases are plotted in figures 5.8.a through 5.8.f. The following observations may be made:

- For cases 2 and 2A, the differences in intensity coefficients between classical plane strain and plane-coupled strain are small. There is no material interface at the corner, and the material coordinates are aligned with the basic coordinate system. However, the nearest ply interface will give rise to out-of-plane deformations and will thus influence the stress level at the corner. For the moment and tension load case, the differences are of the order of 1%; for the shear load case, the differences are of the order of 10%.

- The alternate material (case 2A) exhibits a greater difference. It can be expected that the difference in stresses will be greater the larger the fiber/matrix stiffness ratio.

- For cases 3 and 5, the intensity coefficients are significantly different. Also, the out-of-plane shear stresses are large (of the same order as the other stress components).

The severity of the stress singularity for all stacking orders are summarized in table 5.1. The main difference here is the fact that for classical plane strain the severity is the same for all components and rays, whereas for plane-coupled strain the severity is a function of θ.

5.1.4. Summary

The discussion in this section shows that plane-coupled strain results can differ significantly from classical plane strain results. Also, plane-coupled strain allows for phenomena that do not appear in classical plane strain. The difference in displacement of the overall plate could be small, a point that has not been examined. But locally the differences in stresses are so large that plane-coupled strain should be used for the formulation of any failure criterion.

5.2. The Stress Singularity

5.2.1. Isotropic Test Case and Accuracy of the Solution Method

An isotropic test case, designated as case IS, is used to calibrate the solution method and to judge its accuracy. The test case employs the same geometry and loading conditions as the orthotropic cases, but an isotropic constitutive law is substituted. For a reentrant corner of 90°, free edges and in plane loading (see section 4.2.1.) k can be determined by solving the eigen equation

$$\lambda = \pm \sin(3/2\,\pi\,\lambda)$$

$$k = 1 - \lambda .$$

Thus k is evaluated as k = 0.45552. This value is taken as a reference for the following discussion. The k-values for the composite materials are stated later on as percentage deviations from this reference value.

With a goal of at least 2% accuracy in the determination of k, the required size scale of the finite element mesh at the corner must be found. One must also find a suitable interval over which to fit the straight line on the log-log stress plots in order to determine the k and Ψ_{ij}'s.

The results of the calibration can best be seen by way of an example log-log stress plot, in this case the fiber-normal stresses σ_{ff} of case 2 in tension loading (figure 5.7). The smallest finite elements have edge lengths of 10^{-10} mm. The stresses are accurately resolved to within 10^{-9} mm from the corner. The straight line fit is performed between 10^{-8} and 10^{-6} mm away from the corner. This mesh provides accurate results for the

majority of the cases. Usually, at distances greater than 10^{-4}, the solution deviates significantly from the assumed power law (straight line on log-log scale), due to the vicinity of ply boundaries. As a reference size scale, consider that the next ply interface occurs at about 10^{-1} mm (0.125 to be exact). The number of elements in the radial direction per magnitude is 15. Thus the straight line fit uses 30 data points. Since the intensity coefficients Ψ_{ij} cannot be determined analytically, the correlation of the experimental power k with Williams' solution is used as a guide to the overall accuracy of the solution method.

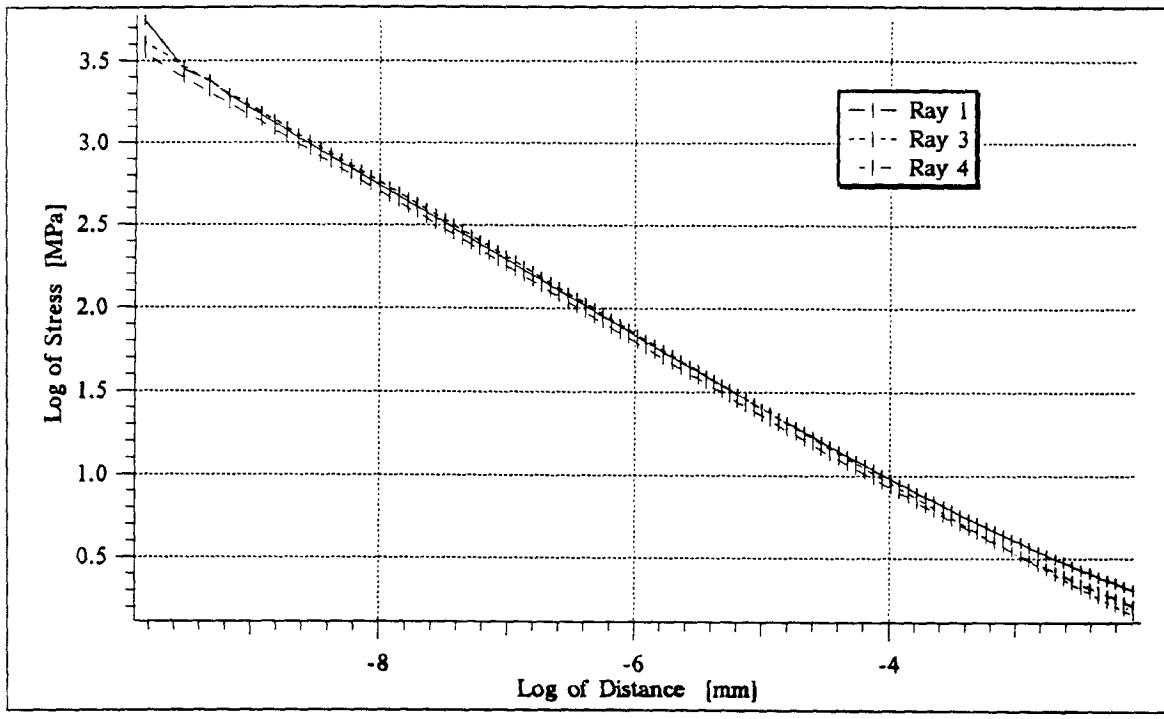

Figure 5.7. Example log-log stress plot; Case 2, Tension, σ_{ff}

For each case a total of 72 values for the intensity coefficients and the severity k are determined. There are six stress components for each of the four rays in the three different load cases. Some of the data must be dismissed because stresses are averaged

across a material interface or should be zero due to a traction free boundary (see section 3.4.).

For the isotropic test case, 36 values for k can be used to gauge the accuracy of the solution method (zero traction on rays 1 and 2, out-of-plane shear stresses identically zero). Twenty-four values fall within 0.5% of the reference value of 0.45552, 9 values between 0.5% and 1.0%, and 3 values between 1.0% and 1.5%. The spread is thought to be equivalent to random experimental scatter, because the solution appears to depend on the boundary conditions and the range used for the straight line fit in a quasi random fashion (similar to computer generated quasi random numbers). Thus, if sufficient data are available, the solution for k can be determined, with some degree of confidence, to within 0.5%. Otherwise, k can be stated to be within 2%. The same degree of accuracy is assumed for the intensity coefficients. However, since the straight line fit is performed on a log-log scale, and the intensity coefficients are stated on a linear scale, the error needs to be converted also. Thus a logarithmic error of 0.5% corresponds to a linear error of 1.1%, and a logarithmic error of 2% corresponds to a linear error of 4.7%.

5.2.3. The Severity of the Singularity

For an isotropic material and a classical plane strain solution, the severity k is a well defined number, valid for all stress components. However, for orthotropic materials and a plane-coupled strain solution, no similar assumptions regarding the severity can be made. The Williams solution is only valid for pure in-plane loading. Figures 5.1. through 5.3 show clearly that out-of-plane deformation occurs locally. It can be expected that the severities are superposition of in-plane and out-of-plane loading results.

Table 5.1.a Severity of the stress singularity, plane-coupled strain

Plate Ply Direction	Stringer Ply Direction	Cases	Major Severity [deviation from isotropic k-value]	Minor Severity [deviation from isotropic k-value]
90	90	1, 2, 2A, 8, 19, 20, 21, 22	3%	27%
90	0	9	7%	-8%
0	90	13, 14, 15, 16, 18	-5.5%	-49%
90	±45	4, 5, 6, 7, 10, 11, 12	3%	7% to 16%
0	±45	17	6%	-6% to -2%
±45	±45	23	-6% to 3%	-4% to 4%
±45	∓45	3	-20% to 2%	-7% to 4%

Table 5.1.b Severity of the stress singularity, classical plane strain

Plate Ply Direction	Stringer Ply Direction	Cases	Severity [deviation from isotropic k-value]
90	90	2R, 2AR	3%
90	±45	5R	7%
±45	∓45	3R	2%

The severity of the singularity appears to be a function of the material orientation for both the plate and stringer material. Table 5.1. is organized according to different interface permutations. The severities are not stated as absolute values, but rather as percentage deviations from the isotropic reference value of 0.45552. In this way, the differences among stacking orders become more apparent. As with most data in the results section,

the stresses are stated in the local material system (x_f, x_m, x_n). For some types of interfaces, either the data were very inconsistent, or only one layup is examined (±45/±45 and ±45/∓45). For the other stacking orders, two distinctly different severities, or groups of severities, have been observed. The one value, called the *major severity*, holds for the normal stresses and one of the shear stresses, usually the in-plane shear. The second value, called the *minor severity*, holds for the remaining two shear stresses, usually the out-of-plane shear components.

The variance in the severities is usually within 1%, and never higher than 2%, for the majority of the cases involving either 0° or 90° plies, and for all the restricted cases (following classical plane strain assumptions). For cases that include ±45° plies, the variance in the severity is much greater. ±45° plies give rise to local out-of-plane loading, and this effect is believed to be responsible for the greater spread in results.

The following statements list interesting phenomena in the above severities. They show the need for further studies into the effects of plane-coupled strain.

- All four classical plane strain cases have only a single severity for all stress components, whereas the corresponding plane-strain solution reveals as least two distinct values. The classical plane strain cases also exhibit relatively small deviations from the isotropic severity k. It may be assumed that the variance in severity is a phenomenon of the assumed displacement field.

- For the cases involving ±45° plies, no pattern in the values of the severities is easily recognizable. For cases with a plate direction of 90° and a stringer direction of ±45°, the variance in the minor value is about ±5%.

It is not clear how the variance in the severity influences the intensity coefficients or a failure criterion. This effect has not been taken into account in the following discussion.

5.2.4. Comparison of Intensity Coefficients

The second component in the characterization of the stress singularity is the intensity coefficients. The intensity coefficients are functions of θ and the applied loads and can be used to compare the expected stresses near the corner between different stacking orders, providing the severity k is constant.

The intensity coefficients are plotted in figures 5.8.a through 5.8.l. The figures present normalized values of the stresses, resolved in the material coordinate system. The material coordinates are chosen because they allow a more descriptive evaluation of the stresses. The values are normalized with respect to one value for all stress components on all rays within each load case. The reference value is arbitrarily taken as the intensity coefficient for σ_{xx} along ray 1 in the isotropic test case IS. The intensity coefficients are plotted as percentages of this reference value.

The six cases with a thicker plate layup, cases 15 through 20, are normalized such that the average stresses through the thickness are equivalent to the stresses in the thinner plates. Thus one obtains a linear relation between the thickness ratio and the applied tension and shear loads, and a quadratic relation between the thickness ratio and the applied moment loads. This normalization of the plate thickness is better suited to a comparison of the global load carrying capabilities of the plate. In order to compare the intensity coefficients between two equivalent geometries (e.g., cases 20 and 21), a different normalization must be used, that takes into account the severity of the stress singularity.

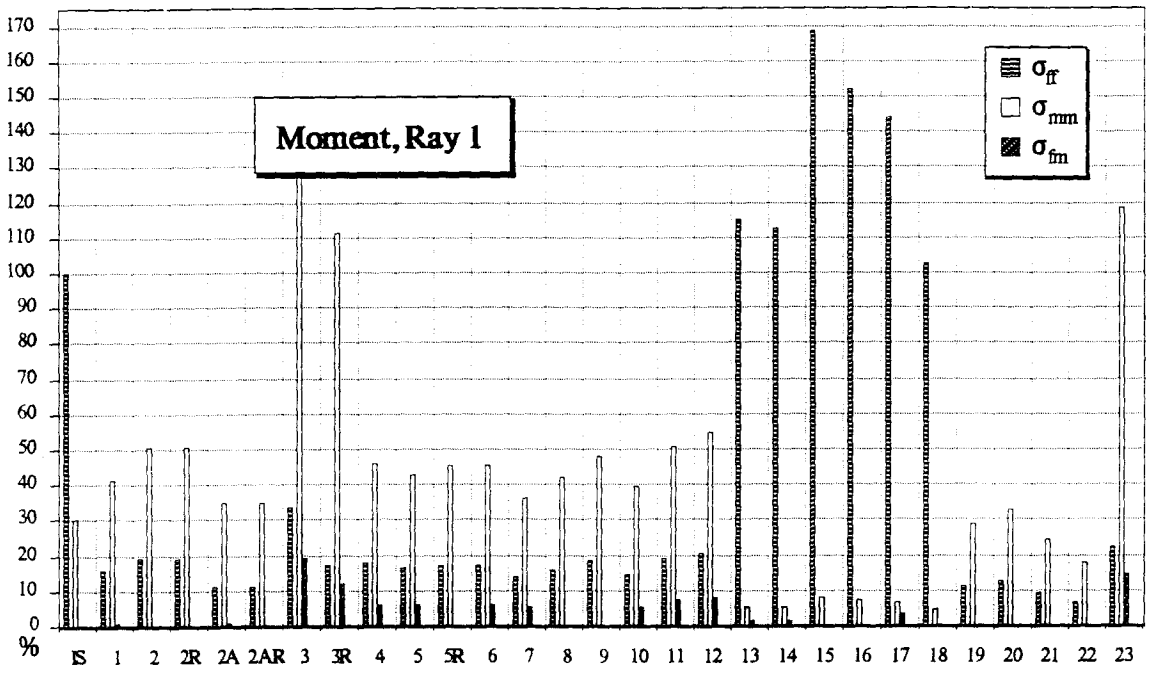

Figure 5.8.a Intensity coefficients; Moment load case, Ray 1

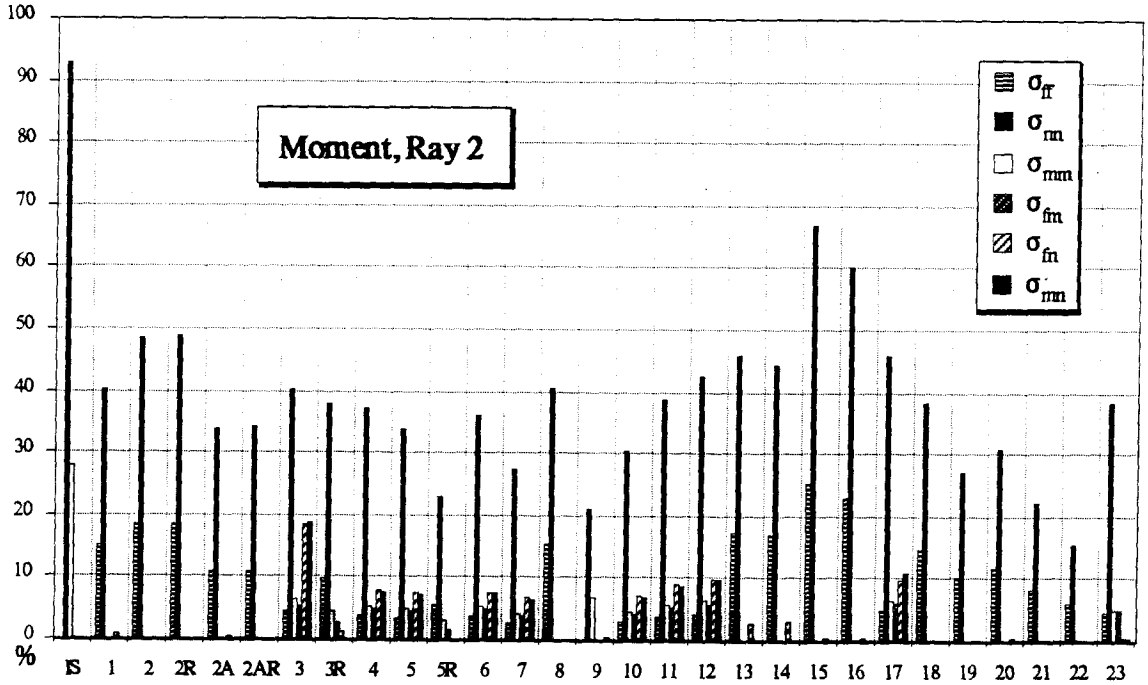

Figure 5.8.b Intensity coefficients; Moment load case, Ray 2

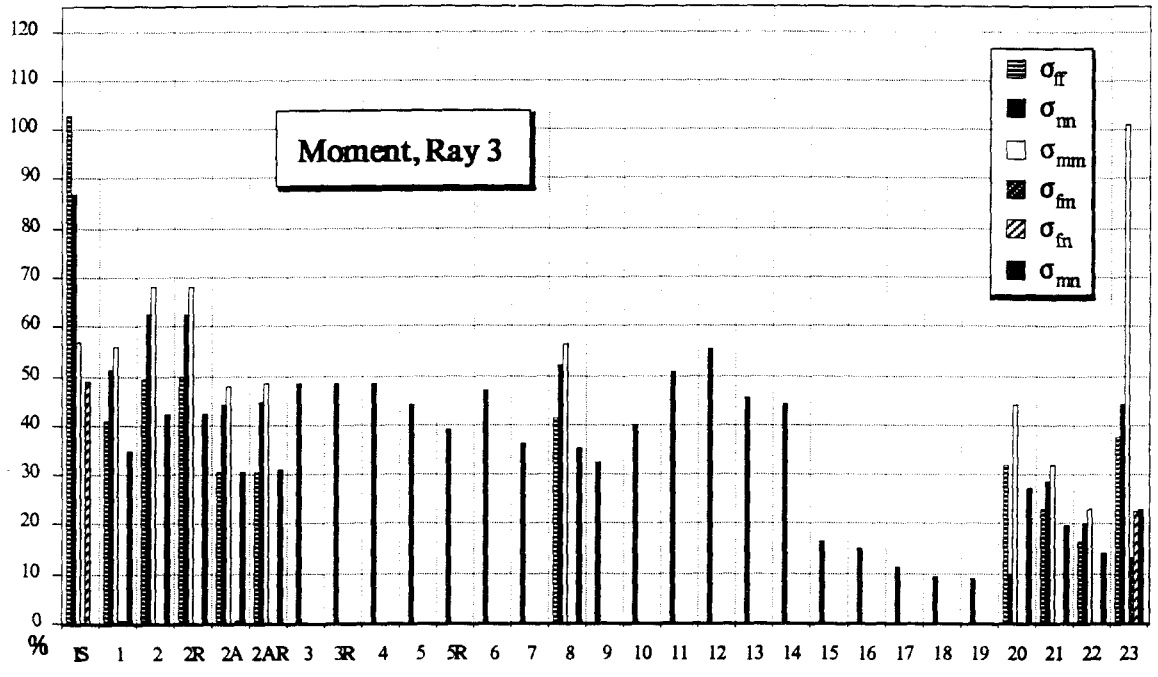

Figure 5.8.c Intensity coefficients; Moment load case, Ray 3

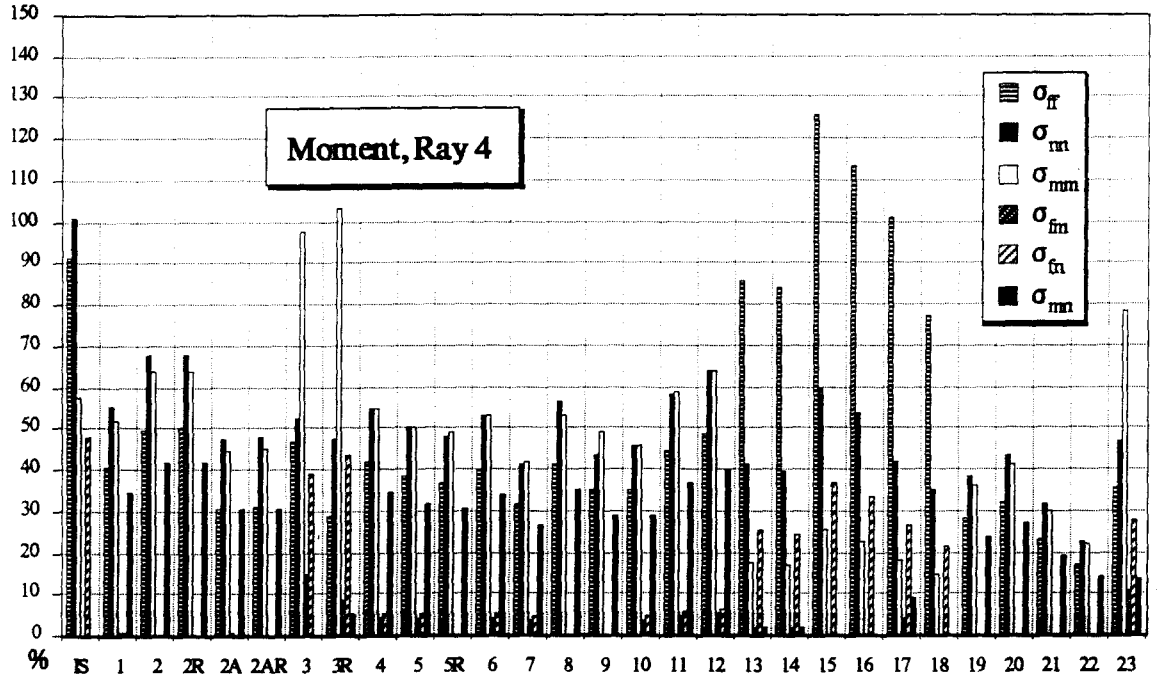

Figure 5.8.d Intensity coefficients; Moment load case, Ray 4

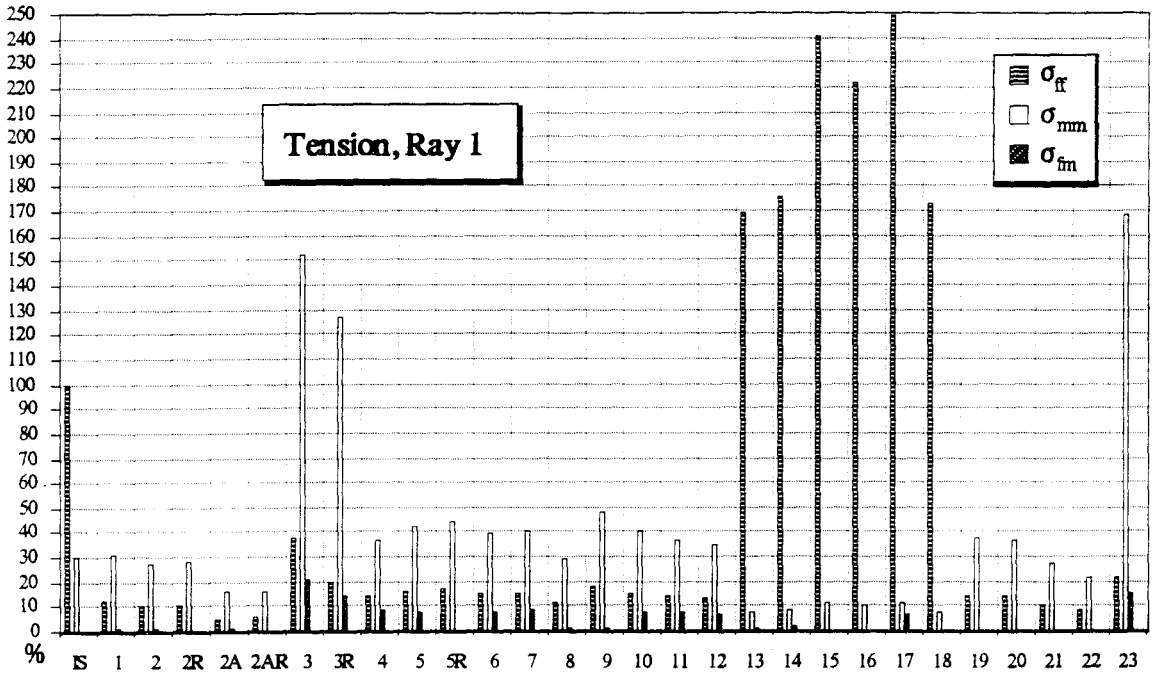

Figure 5.8.e Intensity coefficients; Tension load case, Ray 1

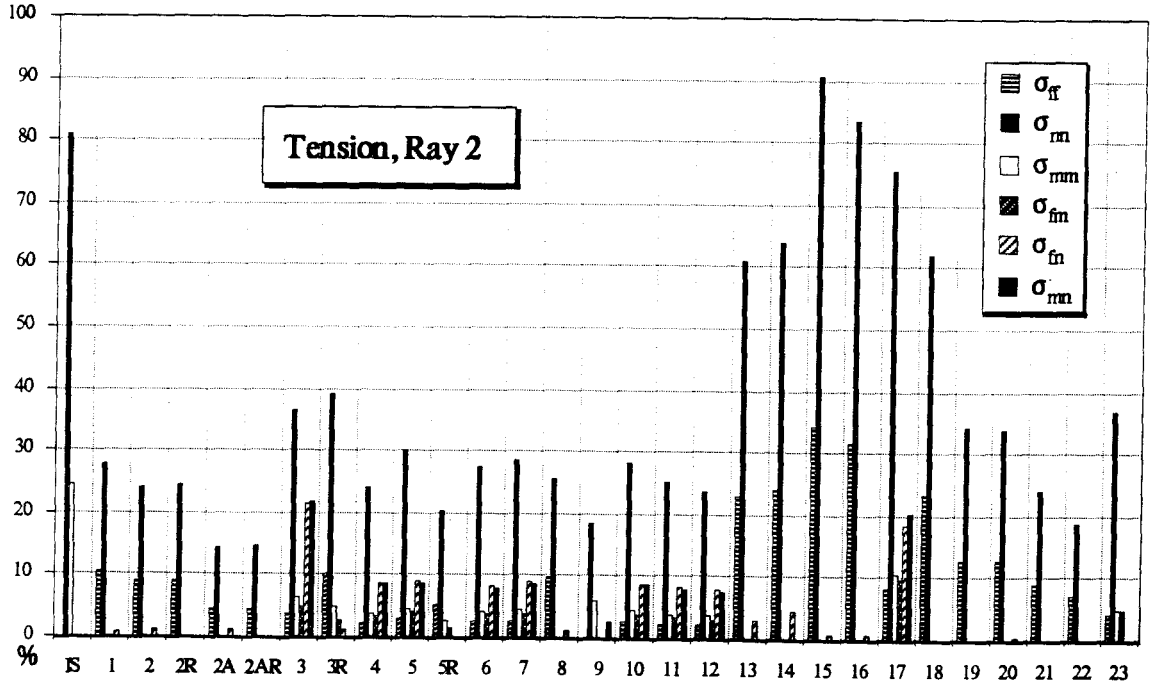

Figure 5.8.f Intensity coefficients; Tension load case, Ray 2

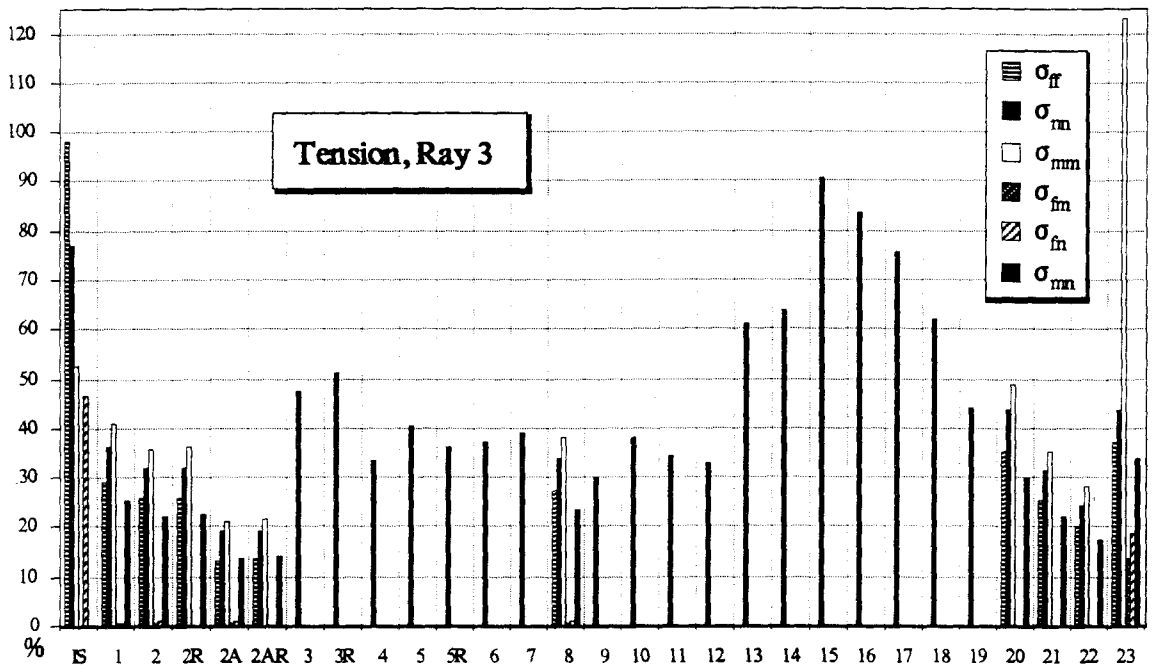

Figure 5.8.g Intensity coefficients; Tension load case, Ray 3

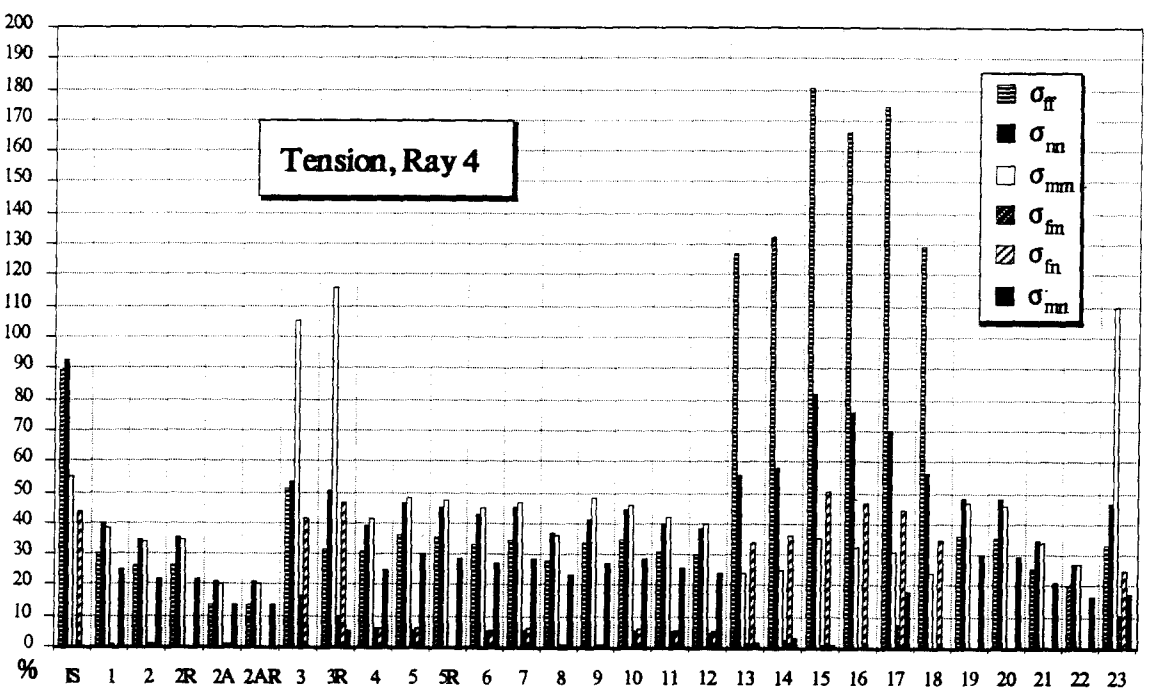

Figure 5.8.h Intensity coefficients; Tension load case, Ray 4

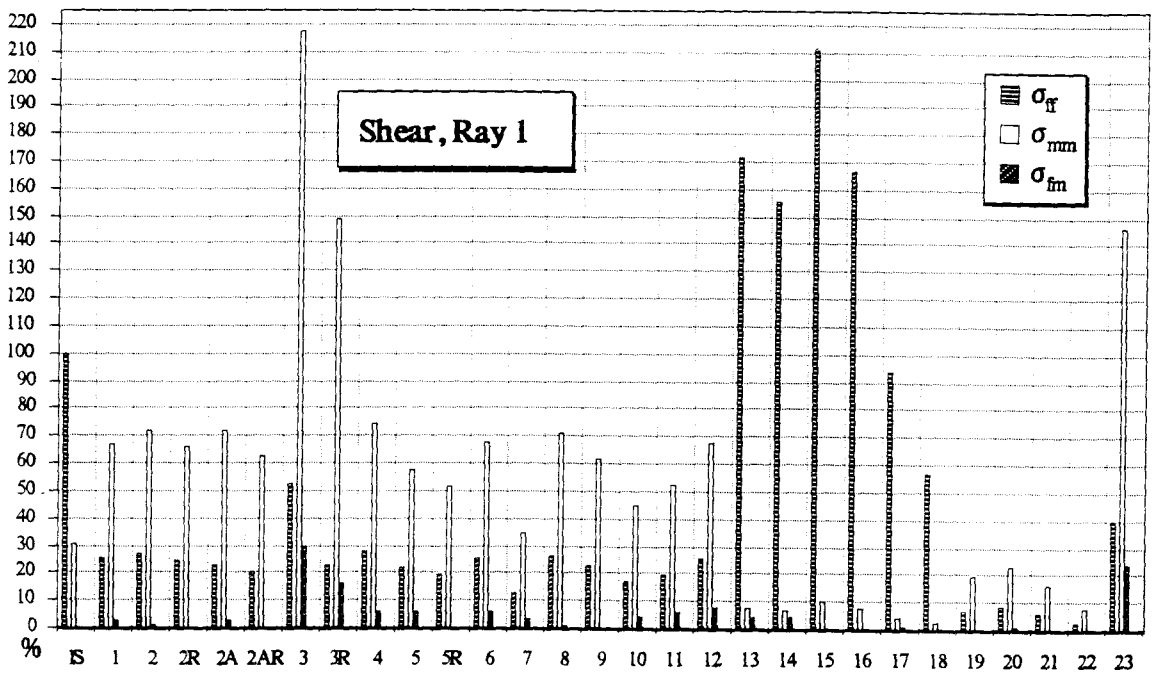

Figure 5.8.i Intensity coefficients; Shear load case, Ray 1

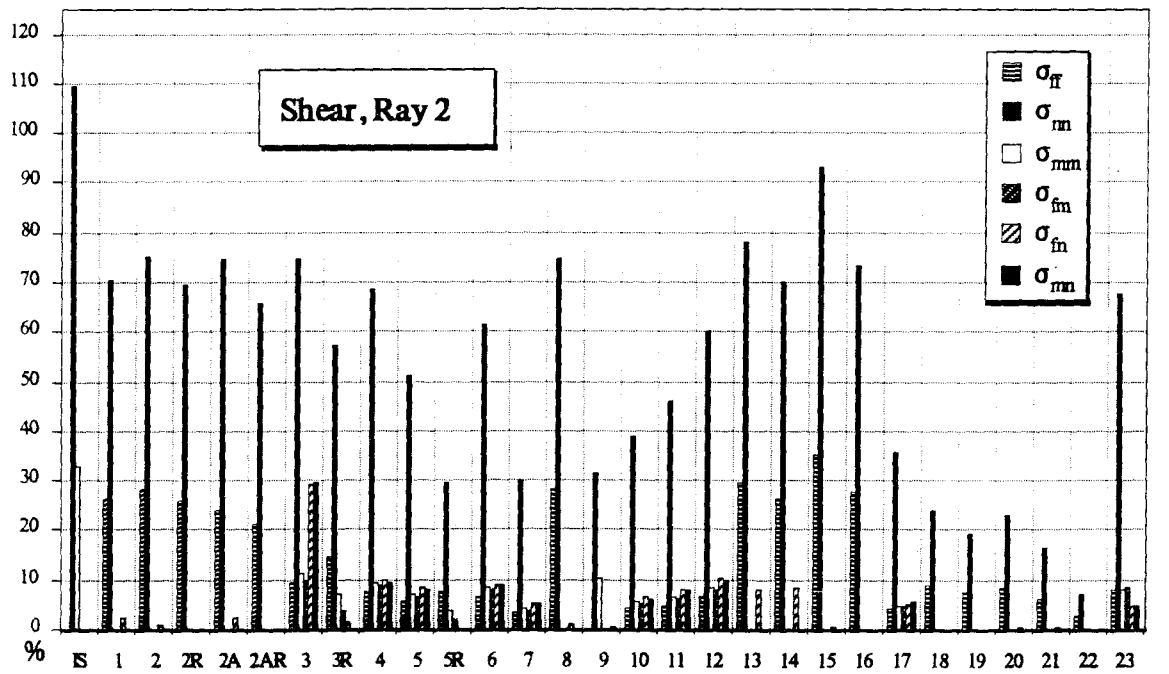

Figure 5.8.j Intensity coefficients; Tension load case, Ray 2

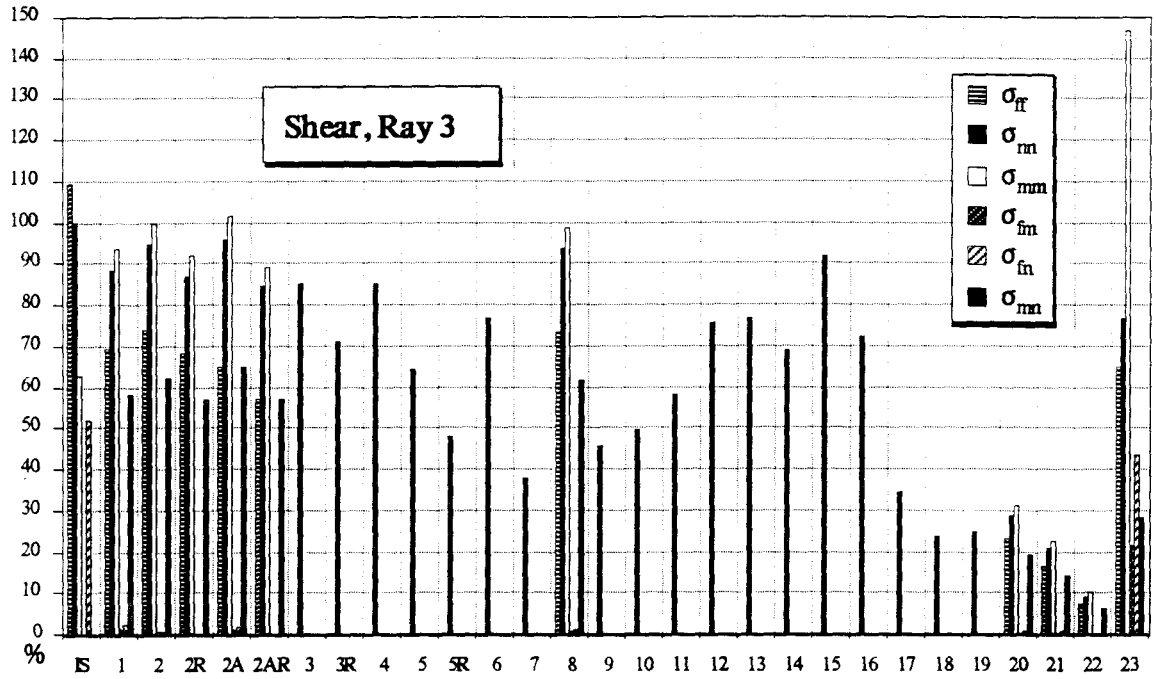

Figure 5.8.k Intensity coefficients; Shear load case, Ray 3

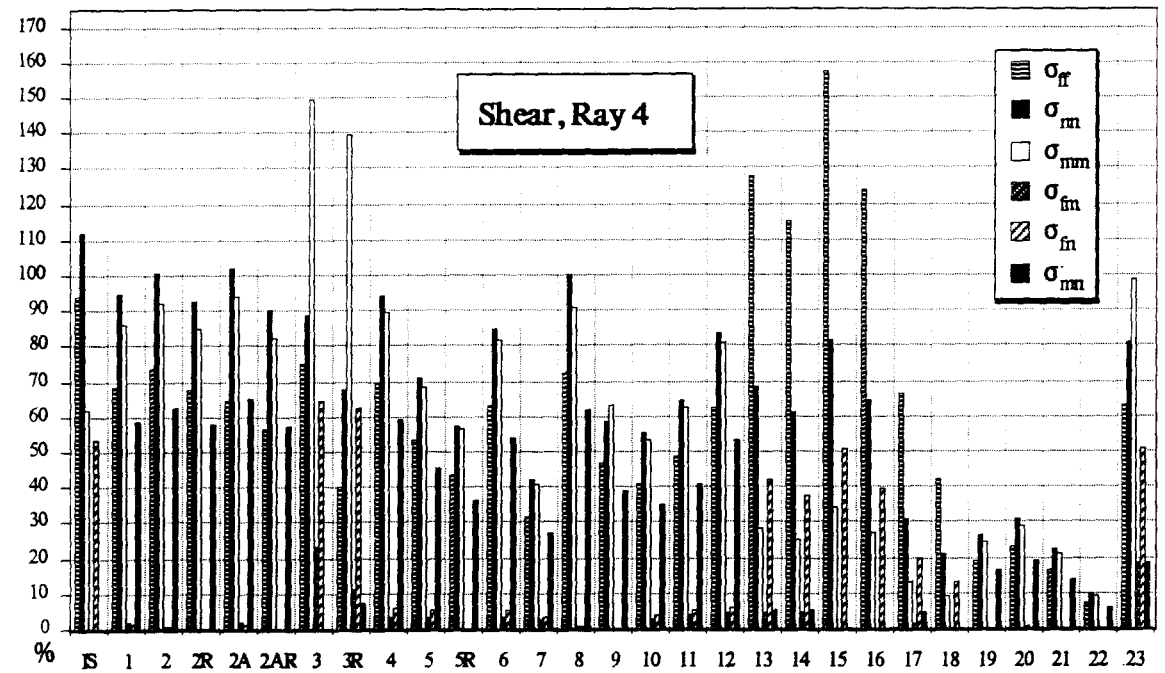

Figure 5.8.1 Intensity coefficients; Shear load case, Ray 4

5.3. Example of a Failure Criterion

This section examines one possible failure criterion using the intensity coefficient found in this study. This example studies the trade-off between the three load cases (moment, tension, and shear) that could lead to delamination at the interface between the plate the the stringer.

Let us assume (on the basis of possible physical reasoning) that the laminate will fail at the interface at the corner if the combined intensity coefficient for σ_{yy} (= σ_{nn}) on ray 3 (interface ray) reaches a critical value. Since the three load cases can be superposed linearly, any linear combination of the intensity coefficients which reaches a critical value will be presumed to result in failure. If we designate this critical intensity coefficient as $\Psi_{crit.}$, the intensity coefficient for the moment case as Ψ_M, for the tension as Ψ_T, and for the shear as Ψ_S, one can then write the condition for failure as:

$$\Psi_M + \Psi_T + \Psi_S \geq \Psi_{crit.}.$$

Consider a three-dimensional space. Let the base vectors be formed by the intensity coefficients of the three load cases (figure 5.9.). We can then plot the above equality as a plane, called the *failure plane*. Any point in the space above the failure plane will result in failure. Let us further define the unit normal to the failure plane as the *failure normal*. The direction of the failure normal can be used to determine the susceptibility of a laminate to failure with respect to the global load cases.

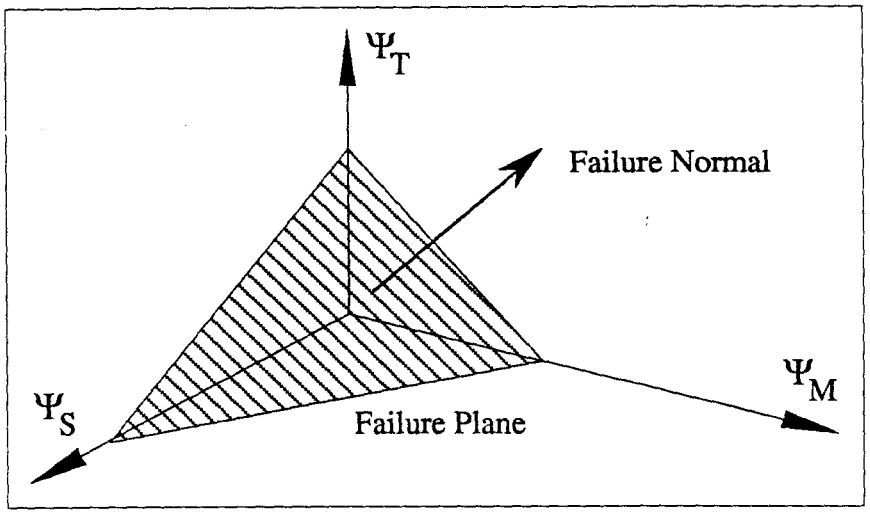

Figure 5.9. Failure plane and failure normal

Figure 5.10. displays the end points of the failure normals for the different stacking orders. The figure is an octaheadral view of the failure space. The octaheadral vector {1,1,1} is perpendicular to the plane of the page. The intensity coefficients have been normalized, such that the failure normal of the isotropic test case IS is parallel to the octaheadral vector, and thus is plotted at the center of the plane, coincident with the origin. The plot only reveals the relation between the contributions of the different load cases and not their absolute values.

In order to aid in the interpretation of figure 5.10., let us look at an example. Consider case 16. The failure normal for case 16 is shifted in the direction of positive tension. This means that the tension-axis intercept of the failure plane occurs at a lower value with respect to the reference case IS. Thus laminate 16 is expected to be more robust in tension than in shear or moment loading.

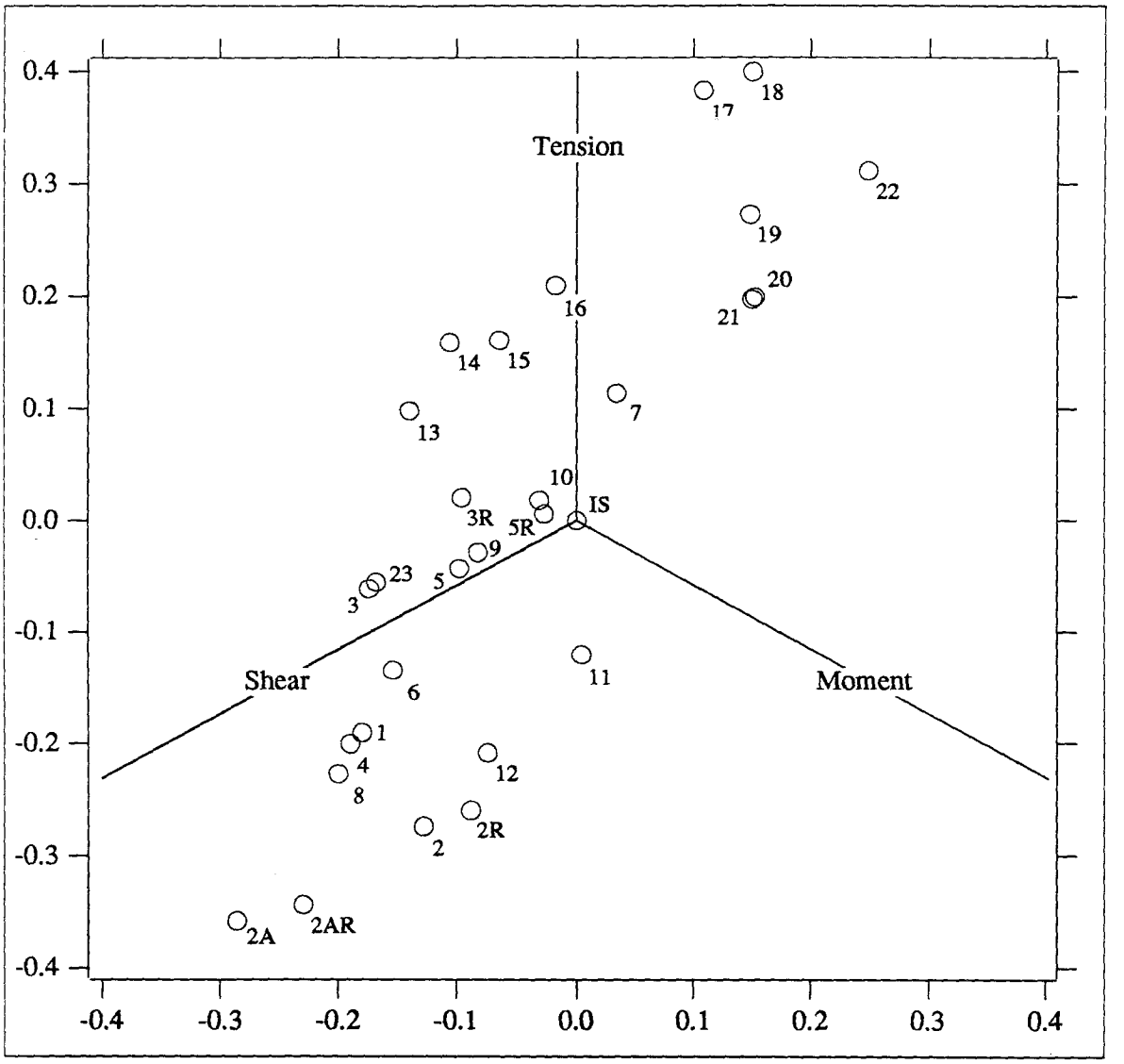

Figure 5.10. End-points of failure normals

It is interesting to note that the use of plane-coupled strain reveals a greater strength in shear than do the corresponding classical plane strain cases. Also, the coincidence of the end points for cases 20 and 21 (case 20 is twice as strong in all geometric dimensions) indicates good convergence of the finite element calculations.

6. Suggestions for Future Research

With these initial results, a host of avenues for continuing research can be taken. This chapter suggests some possible ways to improve and expand on this work.

6.1. Analytical Analysis

The numerical results have shown a number of unexpected phenomena. A closer look at the problem with analytical means may improve the understanding of the physics involved. For example, the relationship between the severity of the stress singularity and plane-coupled strain could be investigated. At this point, it is not clear what factors influence the severity. The introduction of plane-coupled strain also provides for phenomena that are not present in classical plane strain.

6.2. Experimental Work

One main goal of the research program is to predict failure of the structure. In order to allow a prediction via a numerical method, any failure criterion must be calibrated with respect to experimental test results. The test matrix should involve stacking orders with different fiber directions at the reentrant corner. The effect of the fiber direction on failure may be the single most important variable for a failure criterion.

6.3. Improved Numerical Method

The current method of using a solid element to simulate a plane-coupled strain element is not very efficient. The eliminated degrees of freedom do not enter the calculation, but

they still require memory, produce a lot of duplicated data output, and slow the finite element computation. A newly defined plane-coupled strain element would also circumvent the aspect ratio limitations inherent in a problem with vastly differing element sizes.

The possibility of creating a *singularity element* could also be investigated. Such an element would replace the large number of elements currently used to define the stress singularity by incorporating additional degrees of freedom for the severity of the singularity. The element would be similar to a crack tip element.

7. Concluding Remarks

This investigation has attempted to further the understanding of the failure behavior of co-cured, stringer reinforced composite plates. Specifically, the generic problem of a step-down in thickness of a composite plate has been studied, and methods for studying the problem have been developed. Data for several laminate stacking orders have been collected to aid in the development of a possible follow-on experimental investigation.

One goal has been to relate the loads applied on the plate to a local failure criterion. Failure is expected to initiate near the sharp reentrant corner at the step-down. A failure criterion could involve the characteristics of the stress singularity at the corner. The method used to determine characteristics of the stress singularity relies on a fine finite element mesh and produces results that appear reliable to at least 5%. That accuracy seems sufficient to reveal unique phenomena of the step-down geometry in composite structures.

In order to limit the computations, a two-dimensional formulation of the stress field has been sought. The assumed geometry and loading conditions on the plate are such that a plane strain formulation could be used for an isotropic material. However, the use of fiber composite materials requires a more elaborate theory that does not restrict out-of-plane displacements. This theory, called plane-coupled strain, allows an exact two-dimensional stress formulation for in-plane loading conditions. Results obtained for the stresses at the reentrant corner using plane-coupled strain can differ significantly from results obtained with classical plane strain. Plane-coupled strain reveals phenomena that are not observed in classical plane strain. Studies on free-edge delaminations may also benefit from using plane-coupled strain.

The methods have been applied to 23 different stacking sequences. This data base reflects the great variety of possible stacking orders. Failure will depend not only on the applied loads but also on the stacking order. It can be expected that the fiber direction of the material at the reentrant corner will be very important for failure. It is conceivable that a structure can be strengthened by rearranging the stacking sequence without compromising stiffness or cost of manufacture. The data for the different stacking sequences can be used effectively to determine an initial test matrix for a follow-on experimental investigation.

Bibliography

Agarwal, B. D., & Broutman, L. J., "Analysis and Performance of Fiber Composites." John Wiley & Sons, New York, NY, 1980.

Anderson, W. J., "MSC/Nastran Interactive Training Program." John Wiley & Sons, New York, NY, 1983.

Babcock, C.D., Knauss, W.G., & Waas, A.M., "Stress concentrations in composite structures," GALCIT Solid Mechanics Reports SM 83-9, SM 84-17, SM 85-12; California Institute of Technology, Pasadena, CA, 1983-1985.

Cohen, D., and Hyer, M.W., "Calculation of Skin-Stiffener Interface Stresses in Stiffened Composite Panels." Virginia Tech Center for Composite Materials and Structures Report CCMS-87-17 and College of Engineering Report VPI-E-87-32, Blacksburg, Dec. 1987.

Curry, J.M., Johnson, E.R., and Starnes, Jr., J.H., "Effect of ply drop-off on the strength of graphite-epoxy laminate." Virginia Tech Center for Composite Materials and Structures Report CCMS-86-07 and College of Engineering Report VPI-E-86-27, Blacksburg, Dec. 1986.

Fish, John C. & Lee, Sung W., "Tensile Strength of Tapered Composite Structures." University of Maryland, College Park, AIAA Paper 88-2252.

Fish, John C. & Lee, Sung W., "Edge Effects in Tapered Composite Structures." American Helicopter Society, Proceedings, National Technical Specialists' Meeting on Advanced Rotorcraft Structures, October 1988.

Fung, Y. C., "Foundations of Solid Mechanics." California Institute of Technology, Prentice-Hall, Englewood Cliffs, NJ, 1965.

Grimes, G.C. & Dusablon, E.G., "Study of Compression Properties of Graphite/Epoxy Composites with Discontinuities," Composite Materials: Testing and Design (Sixth Conference), ASTM STP 787, I. M. Daniel, Ed. American Society for Testing and Materials, 1982, pp. 513-538.

Jones, R. M., "Mechanics of Composite Materials." Virginia Polytechnic Institute and State University, Blacksburg, Scripta Book Company, Washington, D.C., 1975.

Lekhnitskii, S. G., "Theory of Elasticity of an Anisotropic Elastic Body." Holden-Day, San Francisco, CA, 1963.

Pogue, William R., & Vizzini, Anthony J., "The Effect of Structural Tailoring by Edge Alteration on Free-Edge Delamination", Center for Rotorcraft Education and Research, University of Maryland, College Park. 89A/8887.

Starnes, James H. Jr., Knight, Norman F. Jr., & Rouse, Marshall, "Postbuckling Behavior of Selected Flat Stiffened Graphite-Epoxy Panels Loaded in Compression", NASA Langley Research Center, 23rd Structures, Structural Dynamics and Materials Conference, May 1982. AIAA paper 82-0777.

Timoshenko, S. P., & Goodier, J. N., "Theory of Elasticity," 3rd edition, Stanford University, McGraw-Hill, New York, NY, 1970.

Vinson, J.R., & Chou, T.W., "Composite Materials and their use in structures." University of Delaware, John Wiley & Sons, New York, NY, 1975.

Vinson, J.R., & Sierakowski, R.L., "The Behavior of Structures Composed of Composite Materials." Martinus Nijhoff Publishers, Dordrecht, The Netherlands, 1986.

Waas, A. M., "Compression Failure of Fibrous Laminated Composites in the Presence of Stress Gradients: Experiment and Analysis." Ph.D. Thesis, The California Institute of Technology, Pasadena, CA, 1987.

Wang, J.T.S. & Biggers, S.B., "Skin/Stiffener Interface Stresses in Composite Stiffened Panels," Lockheed-Georgia Company, NASA paper N84-18681, Marietta, GA, 1984.

Williams, M.L., "Stress Singularities Resulting from Various Boundary Conditions in Angular Corners of Plates in Extension," GALCIT, 1952.

Appendix I: Computing Tools

This appendix lists all hard and software products used for this thesis. All products are licensed to either the California Institute of Technology, the Guggenheim Aeronautical Laboratories, or the author.

This work has been performed on two computer systems. Compute intensive tasks have been delegated to a VAX-Cluster (Digital Equipment Corp.). Data reduction and presentation have been mainly performed on an Apple Corp. Macintosh computer system. The following section lists all software products used, including version number, supplier, and the tasks for which they have been used. System software and utilities are not listed separately (operating system, programing languages).

MSC/NASTRAN 66a, The MacNeal-Schwendler Corporation: Finite element calculation.

PATRAN 2.4, PDA Engineering: Pre- and post processing of the finite element data; data reduction.

MACSYMA, Symbolics Inc.: Manipulation of matrices (constitutive law).

Igor 1.12, WaveMetrics: Data processing, reduction and presentation; curve fitting (stress singularity).

MathType 2.10, Design Science, Inc.: Presentation.

Microsoft Word 4.0, Microsoft Corporation: Data reduction; presentation.

Microsoft Excel 2.2, Microsoft Corporation: Data processing and reduction.

MacDraw II 1.1, Claris Corporation: Presentation.

Cricket Graph 1.3, Cricket Software: Presentation.

VersaTerm-Pro 3.0, Abelbeck Software: Terminal emulation; data transfer.

Appendix II: Implementation of Plane-Coupled Strain in Nastran

There are two options available to implement the plane-coupled strain in a finite element solution. The first option involves the definition of a new element. The second option uses a standard three-dimensional element and constrains it properly to obtain the desired properties. The second option is used in this investigation. This appendix describes the implementation of plane-coupled strain in MSC/NASTRAN. The reader is expected to be familiar with the code and its nomenclature. For a generic description of plane-coupled strain consult section 4.1. of the main text. A short Fortran program was written to convert a two-dimensional mesh into a mesh suitable for plane-coupled strain. A program listing is not provided here, but rather some of the techniques used are presented.

It is best to start with a fully functional input deck for a two-dimensional analysis. The Fortran program then converts all two-dimensional elements into solid elements and applies appropriate constraints on them. It will then be necessary to supply the converted data deck with appropriate element property cards (including material and coordinate cards). Applied loads may need to be modified since the plane-strain model does not necessarily have unit thickness. All other cards can be used as is (SPC, GRDSET, PARAM, etc.).

Two-dimensional elements are converted into their 3-D equivalents according to the following table.

CQUAD4	-->	CHEXA (with 8 nodes)
CQUAD8	-->	CHEXA (with 16 nodes)
CTRIA	-->	CPENTA

To convert the solid elements to plane-coupled strain elements, constraints are applied using multipoint constraint cards (MPC1). See also section 4.1.4. Three MPC1 cards are necessary for each node of the two-dimensional deck.

Each node of the two-dimensional model is duplicated. The original node is called the primary node, the duplicated one the secondary node. The secondary node is positioned at the same x and y coordinates as the primary but offset in the z-direction by the slab thickness t. It is convenient to have all secondary node identification numbers offset by an equal amount (which must be higher than the largest primary node identification number). This way is becomes easy to determine the connectivity of the solid elements. It is possible to prescribe a known and constant z-strain by adding a scalar grid SPOINT and including it in the MPC1-card for the z-displacement. This option is not used in this investigation. It is assumed that the plate problem uses different property identification entries to distinguish between different plies. New property cards must be provided for the solid elements.

Because all elements of the new deck must have the same thickness, one can have difficulties with respect to aspect ratio limitations of the elements. MSC does not recommend aspect ratios which exceed 100 for the solid elements. This limitation would restrict the ratio of the longest to the smallest element edge in the plate problem to 10000. However, for nearly rectangular elements, this limit can be increased. For this work, aspect ratios of up to 1000 have been used for nearly rectangular elements without noticeable degradation in element performance.